Tectonophysics 541-543 (2012) 1–18

Contents lists available at SciVerse ScienceDirect

Tectonophysics

journal homepage: www.elsevier.com/locate/tecto

Low temperature thermochronology in the Eastern Alps: Implications for structural and topographic evolution

Andreas Wölfler [a,*], Kurt Stüwe [a], Martin Danišík [b,c], Noreen J. Evans [b,d]

[a] Institute of Earth Sciences, University of Graz, Universitätsplatz 2, 8010 Graz, Austria
[b] John de Laeter Centre for Isotope Research, Applied Geology, Curtin University of Technology, GPO Box U1987, Perth WA 6845, Australia
[c] Departement of Earth & Ocean Sciences, Faculty of Science & Engineering, University of Waikato, Hillcrest Road, Hamilton, New Zealand
[d] CSIRO Earth Science and Resource Engineering, ARRC, 26 Dick Perry Avenue, WA 6151, Australia

ARTICLE INFO

Article history:
Received 10 August 2011
Received in revised form 26 February 2012
Accepted 10 March 2012
Available online 20 March 2012

Keywords:
Eastern Alps
Tauern Window
Fission track dating
(U–Th)/He dating
Fault activity
Isotherms

ABSTRACT

According to new apatite fission track, zircon- and apatite (U–Th)/He data, we constrain the near-surface history of the southeastern Tauern Window and adjacent Austrolapine units. The multi-system thermochronological data demonstrate that age-elevation correlations may lead to false implications about exhumation and cooling in the upper crust. We suggest that isothermal warping in the Penninic units that are in the position of a footwall, is due to uplift, erosion and the buildup of topography. Additionally we propose that exhumation rates in the Penninic units did not increase during the Middle Miocene, thus during the time of lateral extrusion. In contrast, exhumation rates of the Austroalpine hangingwall did increase from the Paleogene to the Neogene and the isotherms in this unit were not warped. The new zircon (U–Th)/He ages as well as zircon fission track ages from the literature document a Middle Miocene exhumation pulse which correlates with a period of enhanced sediment accumulation during that time. However, enhanced sedimentation- and exhumation rates at the Miocene/Pliocene boundary, as observed in the Western- and Central Alps, cannot be observed in the Eastern Alps. This contradicts a climatic trigger for surface uplift, and makes a tectonic trigger and/or deep-seated mechanism more obvious to explain surface uplift in the Eastern Alps.
In combination with already published geochronological ages, our new data demonstrate Oligocene to Late Miocene fault activity along the Möll valley fault that constitutes a major shear zone in the Eastern Alps. In this context we suggest a geometrical and temporal relationship of the Katschberg-, Polinik–Möll valley- and Mur–Mürz faults that define the extruding wedge in the eastern part of the Eastern Alps. Equal deformation- and fission track cooling ages along the Katschberg–Brenner- and Simplon normal faults demonstrate overall Middle Miocene extension in the whole alpine arc.

1. Introduction

Crustal scale fault zones play an important role in the evolution of orogens, both during continental collision and subsequent extension (e.g. Selverstone, 2005). In the Eastern Alps, northward oblique indentation of the European continent by a semi-rigid crustal block (the so-called Adriatic indenter) (Ratschbacher et al., 1991a,b; Rosenberg et al., 2007) caused lateral extrusion of the orogen during the collisional stage, accommodated along major faults. However, it is not clear if this extrusion occurred in a regime of extension or compression (Robl and Stüwe, 2005a,b) and the fault zones provide evidence for both: Major west–east striking conjugate strike slip zones apparently formed in a regime of compression (Fig. 1) and north–south striking detachments around the tectonic windows formed in a regime of east–west extension. Unfortunately, the temporal relationship between the west–east oriented strike slip zones and north–south detachments is not very well resolved. Some of the west–east striking fault zones were activated by at least Middle Oligocene times (Glodny et al., 2008) and continued to be active throughout the Neogene (Reinecker and Lenhardt, 1999) when the detachments were active (e.g. Fügenschuh et al., 1997; Wölfler et al., 2008). However, the geochronological data that document this activity are from exhumed mylonitic shear zones (e.g. Glodny et al., 2008 and references therein) and therefore reflect displacements under ductile conditions. Data related to the cataclastic shear zones that form the majority of the fault zones in the Eastern Alps are rare. These data demonstrate Oligecene to Early Miocene fault activity to the southeast of the Tauern Window (Kralik et al., 1987) and Late Miocene to Pliocene fault activity along the Pöls–Lavanttal fault system (Fig. 1) in the eastern part of the Eastern Alps (Wölfler et al., 2010).

1.1. Fault zones bounding the Tauern Window

The Tauern Window plays a critical role in the recent evolution of the Eastern Alps. The Tauern Window is bound by the north–south

* Corresponding author at: Institute of Earth Sciences, University of Graz, Universitätsplatz 2, A 8010 Graz, Austria. Tel.: +43 316 380 8714; fax: +43 316 380 9865.
E-mail address: andreas.woelfler@uni-graz.at (A. Wölfler).

0040-1951/$ – see front matter © 2012 Elsevier B.V. All rights reserved.
doi:10.1016/j.tecto.2012.03.016

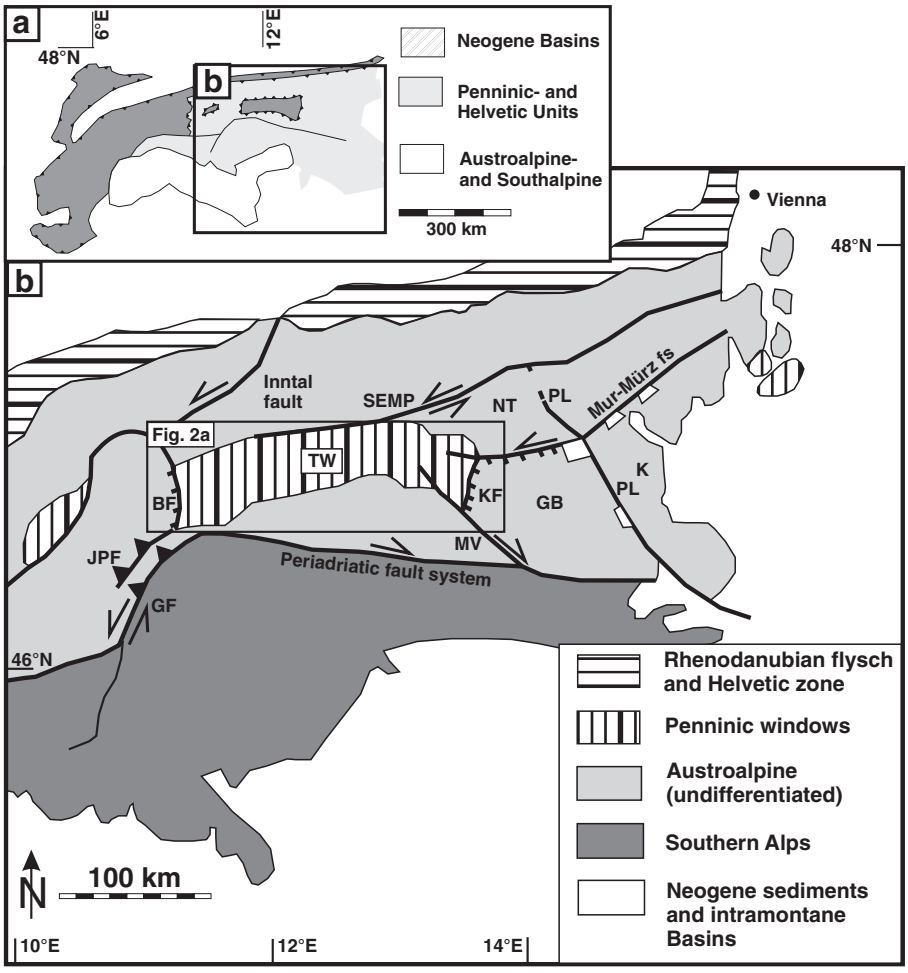

Fig. 1. (a) Simplified tectonic sketch map of the European Alps. (b) Geological sketch map of the Eastern- and Southern Alps. BF: Brenner normal fault; KF: Katschberg normal fault; GF: Giudicarie fault; JPF = Jaufen–Passeier fault; SEMP: Salzach–Ennstal–Mariazell Puchberg fault system; PL: Pöls–Lavanttal fault system; Mur–Mürz fs: Mur–Mürz fault system; MV: Möll valley fault; TW: Tauern Window; NT: Niedere Tauern; GB: Gurktal Block (Gurktal Alps); K: Koralpe.

striking Brenner normal fault (or detachment) (Selverstone, 1988) in the west and the Katschberg normal fault (Genser and Neubauer, 1989) in the east and exposes rocks from the Penninic domain of the Alps (Fig. 1). To the north the Tauern Window is bordered by the Salzach–Ennstal–Mariazell Puchberg fault zone (termed SEMP) (Fig. 1). Recent studies demonstrate that the SEMP truncates into the western part of the Tauern Window within a 50 km long mylonitic belt (Rosenberg and Schneider, 2008). Detailed kinematic analysis reveals sinistral slip (Decker and Peresson, 1996; Linzer et al., 1997; Wang and Neubauer, 1998) accommodating a displacement of 60 km (Linzer et al., 1997, 2002) during Oligocene and Miocene times.

The southern boundary of the Eastern Alps is represented by the Periadriatic fault system (Fig. 1). This is the most prominent fault zone in the European Alps, separating the Soutalpine form the Austroalpine units (Fig. 1). While the Periadriatic fault system to the south of the Tauern Window generally strikes E–W, it forms a complex system of SW–NE striking strike slip-, normal- and reverse faults to the SW of the Tauern Window (Fig. 1) (e.g. Schmid et al., 1989; Viola et al., 2001).

Between the Tauern Window and the Periadriatic fault system, a series of major fault zones form an anatomising network of faults with different senses of displacement. Northwest striking faults with dextral displacement include the Möll valley fault and the Polinik fault to the southeast of the Tauern Window (Fig. 2a). Northeast striking faults with sinistral displacement include the Defereggen–Antholz–Vals fault system and the Zwischenbergen–Wöllatratten fault and its eastern continuation, the Moser fault (Fig. 2a). The Defereggen–Antholz–Vals fault represents a ~80 km long northeast striking fault with sinistral displacement during the Oligocene (Mancktelow et al., 2001; Müller et al., 2000). It consists of mylonites that are, particularly in the eastern part, accompanied and overprinted by semi-brittle and cataclastic shearing (Schulz, 1989). The Zwischenbergen–Wöllatratten fault acts as a synthetic riedel to the Defereggen–Antholz–Vals fault system (Linner et al., 2008). The Möll valley fault forms a subvertical topographic and structural lineament with a total length of ~100 km (Fig. 1) that was mainly active in the Early to Middle Miocene (Wölfler et al., 2008). The Polinik fault is characterized by both ductile strike slip and brittle dip slip displacement (Hoke, 1990) (Fig. 2a).

Selverstone (2005) argued that the exhumation of the Tauern window along its western bound — the Brenner normal fault — is mechanically implausible, unless the Brenner normal fault is directly connected with the west–east striking strike slip zones to the north and south of the window (Fig. 1) — the Inntal fault in the north and the Periadriatic fault system in the south. This suggestion was confirmed by Robl et al. (2008) using numerical modeling. Within this interpretation, the Brenner detachment itself may not necessarily indicate horizontal extension and may simply relate to the compressive tectonically forced extrusion regime. A similar situation exists along the eastern margin of the Tauern Window: The north–south striking Katschberg normal fault is geometrically linked with the Möll valley fault in the south and possibly with the Mur–Mürz fault system in the north (Wölfler et al., 2011) (Fig. 1). This geometric association nourishes the suspicion that the extensional detachment

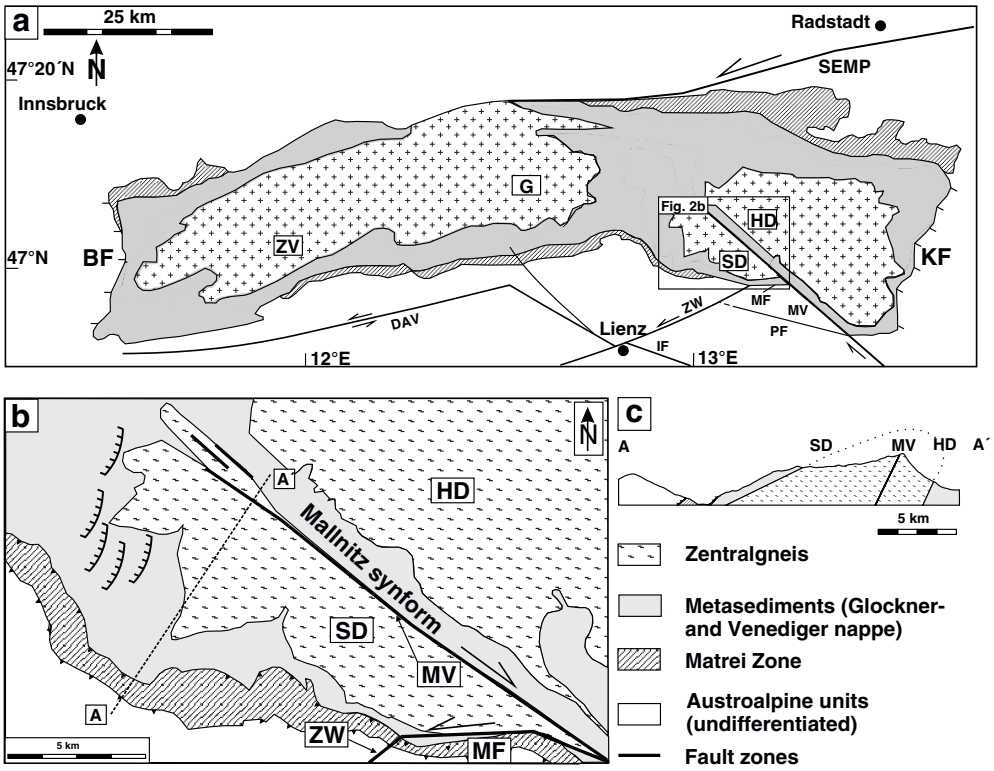

Fig. 2. (a) Simplified geological map of the Tauern Window. (b) Simplified geological map of the study area. (c) Profile that shows the north-east vergent antiformal dome structure of the Sonnblick Dome. SEMP: Salzach–Ennstal–Mariazell Puchberg fault system; ZV: Zillertal Venediger Domes; G: Granatspitz Dome; SD: Sonnblick Dome; HD: Hochalm Dome; BF: Brenner normal fault; KF: Katschber normal fault; DAV: Defereggen–Antholz–Vals fault; ZW: Zwischenbergen–Wöllatratten fault; PF: Polinik fault; MV: Möll valley fault; MF: Moser fault; IF: Iseltal fault; profile A–A′ see also Fig. 3.

is genetically linked to the extruding strike slip zones. However, the temporal relationship between the activities of these different fault zones at the eastern margin of the window is barely known.

1.2. Topographic evolution of the Eastern Alps

Since decades, the topographic evolution of the European Alps is a much debated topic. Since the Oligocene, in the course of collision and slab breakoff the Alps were uplifted and formed a mountain range (e.g. Frisch et al., 1998; von Blanckenburg and Davis, 1995). Temporary rises of sediment flux into the foreland basins occurred between ~24 and ~22 Ma during thrust loading and between ~18 and ~15 Ma as response to axial updoming of core complexes (e.g. Tauern Window) (Fig. 1) (Kuhlemann, 2007). Fission track data as well as sediment budget data independently suggest an increase of both the exhumation rates and the sediment flux at ~5 Ma (Kuhlemann, 2000; Vernon et al., 2008)). On the regional scale, however, the increase in exhumation rate is not evident or occurred at different time (e.g. Bogdanoff et al., 2000; Glotzbach et al., 2008). In contrast to the Western- and Central Alps an increase in exhumation rates at ~5 Ma is not recorded in fission track data of the Eastern Alps (Luth and Willingshofer, 2008). However, surface uplift since, ~6 Ma has been observed in the Eastern Alps too (Genser et al., 2007).

Several potential drivers for this "5 Ma event" have been discussed: (i) isostatic rebound due to climate-triggerd accelerated erosion (Cederbom et al., 2004, 2011), (ii) climate change coeval with backstepping of the active deformation front (Willett et al., 2006), (iii) tectonic underplating (Mosar, 1999), (iv) mantle upwelling (Lyon-Cean and Molnar, 1989), (v) mantle delamination (Kissling et al., 2006), (vi) crustal overthickening (Burg et al., 2002; Genser et al., 2007).

As pointed out by Frisch et al. (1998) the topographic evolution of the Eastern Alps differs significantly from those in the Western- and Central Alps. Especially to the east of the Tauern Window marine deposits of at least Early Miocene age are still preserved (Dunkl et al., 2005; Frisch et al., 2000; Kuhlemann et al., 2001; Winkler-Hermaden, 1957). These areas, the Gurktal- and Koralpe (Fig. 1), are characterized by very low erosion- (Hejl, 1997) and incision rates in the order of 0.1 mm/y over the last 4 Ma (Wagner et al., 2010).

Moreover, palinspastic reconstructions (Frisch et al., 1998) and thermochronological studies (Foeken et al., 2007) demonstrate that present-day topography in the Tauern Window developed already in Middle- to Late Miocene times and exhumation rates did not increase dramatically since that time (Wölfler et al., 2008).

In this study we reconstruct the ductile to brittle evolution of the Möll valley fault (Fig. 2) in order to place constraints on the relative chronology of structures bounding the Tauern Window. Previous geochronological studies have demonstrated different temporal evolution to the south and north of the Möll valley fault (Figs. 3, 4a) (Reddy et al., 1993; Wölfler et al., 2008). Based on apatite fission track (AFT) — and apatite (U–Th)/He (AHE) — age-elevation profiles and thermal history modeling Wölfler et al. (2008) suggested that fault activity along the Möll valley fault occurred in the Late Miocene and Pliocene, between 10 and 5 Ma. However, these data are from profiles that are 20 km apart and do not cross the fault zone itself.

We present new apatite fission track (AFT), zircon (U–Th)/He (ZHE) and apatite (U–Th)/He (AHE) ages along a 25 km long profile that crosses the border of the Austroalpine and Penninic units as well as the Möll valley fault (Fig. 2b, c). Our data are used to test possible differences in thermal evolution on each side of the Möll valley fault and the closure temperatures of these thermochronometers can be used to infer vertical motions in the brittle regime of the upper crust. The new data is then considered in a broader context to constrain the genetic link between the detachments and the strike slip zones and their mechanical relevance for exhumation in the Eastern Alps during the Miocene.

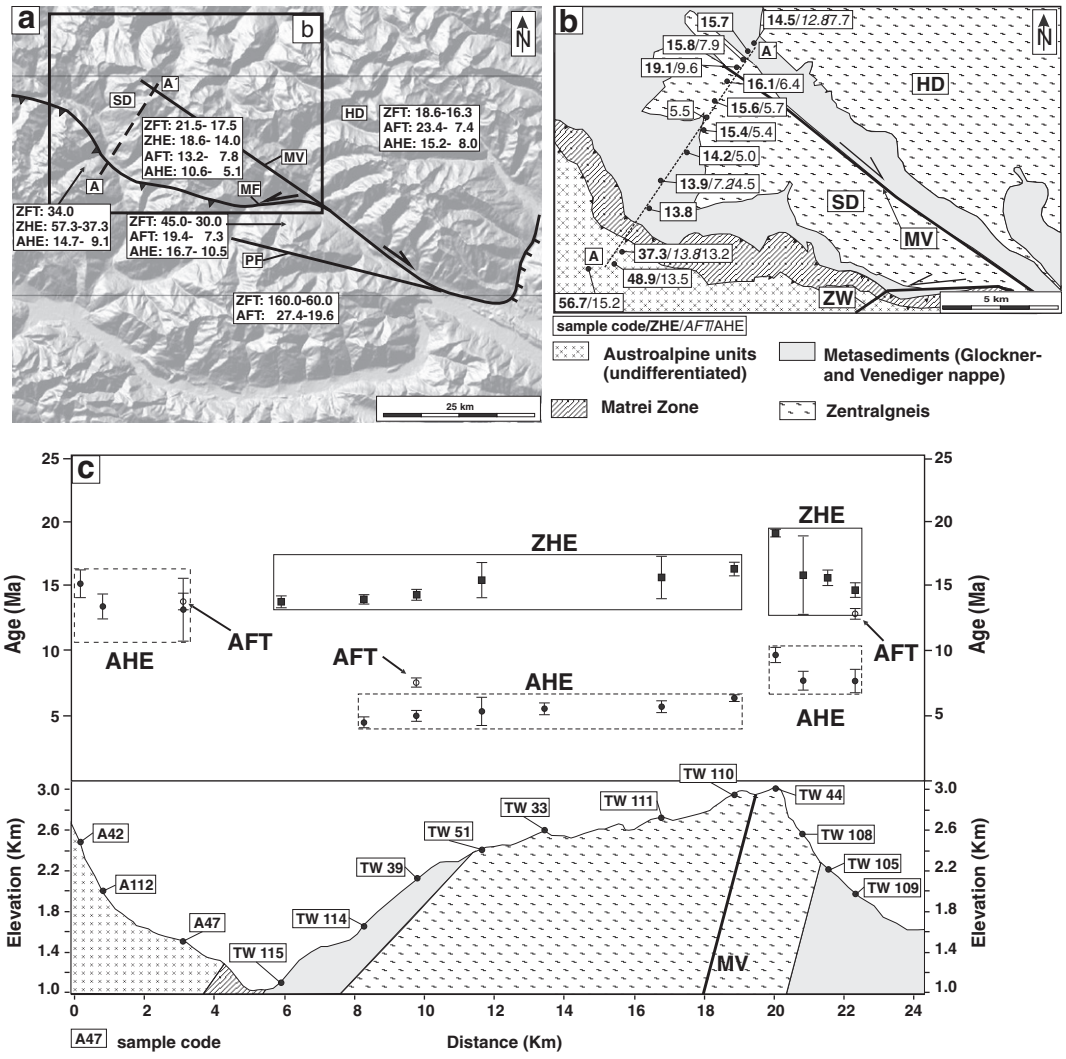

Fig. 3. (a) Digital elevation model with new and published thermochronological ages of the southeastern Tauern Window and adjacent Austroalpine units. Data are from: ZFT: Dunkl et al. (2003); ZHE: this study; AFT: Foeken et al. (2007), Staufenberg (1987), Wölfler et al. (2008), this study; AHE: Foeken et al. (2007), Wölfler et al. (2008), this study; SD: Sonnblick Dome; HD: Hochalm Dome; MV: Möll valley fault; PF: Polinik fault; MF: Moser fault; (b) Geological map of the study area, with sample locations and new thermochronological ages; SD: Sonnblick Dome; HA: Hochalm Dome; MV: Möll valley fault; (c) Topography with sample codes and apatite fission track — (AFT), zircon — (ZHE) and apatite (U–Th)/He (AHE) ages along profile A to A′ (see Fig. 2b); boxes with bold line: range of ZHE ages; boxes with dashed line: range of AHE ages; black squares: ZHE ages; white circles: AFT ages; black circles: AHE ages.

In order to contribute to the discussion of accelerated sedimentation–exhumation rates during Miocene and Pliocene times, we compare our new data and already published ZFT, AFT and AHE data with rates of sediment production from the Alps (Kuhlemann, 2000; Kuhlemann et al., 2002; Willett, 2010). The aim is to understand, if apparent increase in sediment flux can be correlated with an increase in exhumation rates and possibly with surface uplift and the formation of topography.

2. Geological setting

In the Eastern Alps, the tectonic units that originate from the Penninic domain are widely buried beneath the Austroalpine nappe complex, formerly part of the Mesozoic Adriatic plate (Fig. 1). The overthrusting of the Austroalpine nappes over the rocks of the Penninic ocean floor occurred throughout the Cretaceous and lasted until the Eocene (e.g. Kurz et al., 2001). During the later lateral eastward extrusion of the Eastern Alps towards the Pannonian basin, north–south striking detachments developed that successively opened the Tauern Window in a west–east direction, re-exposing the Penninic rocks (Frisch et al., 1998). Kinematic evidence for the Miocene stress field and exhumation processes in the Austroalpine units is confined to discrete structures as much of the Austroalpine units resided in the brittle part of the crust at this time (e.g. Ratschbacher et al., 1991b). Today, the southeast corner of the Tauern window represents a key locality to reveal past tectonic evolution, as the Austroalpine units, the Penninic basement- and cover units and the bounding detachment and strike slip structures are all exposed in close spatial proximity.

To the northeast and east, the Tauern Window is bordered by the Niedere Tauern and the Gurktal Block that represent polymetamorphic Austroalpine units (Fig. 1). The Austroalpine units to the south of the Tauern Window largely consist of pre-Variscan rocks that were affected by Variscan, Permian and later Cretaceous metamorphism during the Eoalpine orogeny (e.g. Schuster and Stüwe, 2008; Thöni, 2006). In the study area, the Eoalpine metamorphic imprint extends to amphibolite and eclogite facies (e.g. Hoke, 1990; Schuster et al., 2001; Thöni, 2006).

The Penninic domains are exposed inside the Tauern Window (Figs. 1, 2a), constituting an exhumed section of the Penninic nappe stack that developed in a collision zone subsequent to closure of the Penninic ocean in the Late Cretaceous and Paleogene (e.g. Kurz et al., 2001). These units consist of a Variscan basement nappe, the

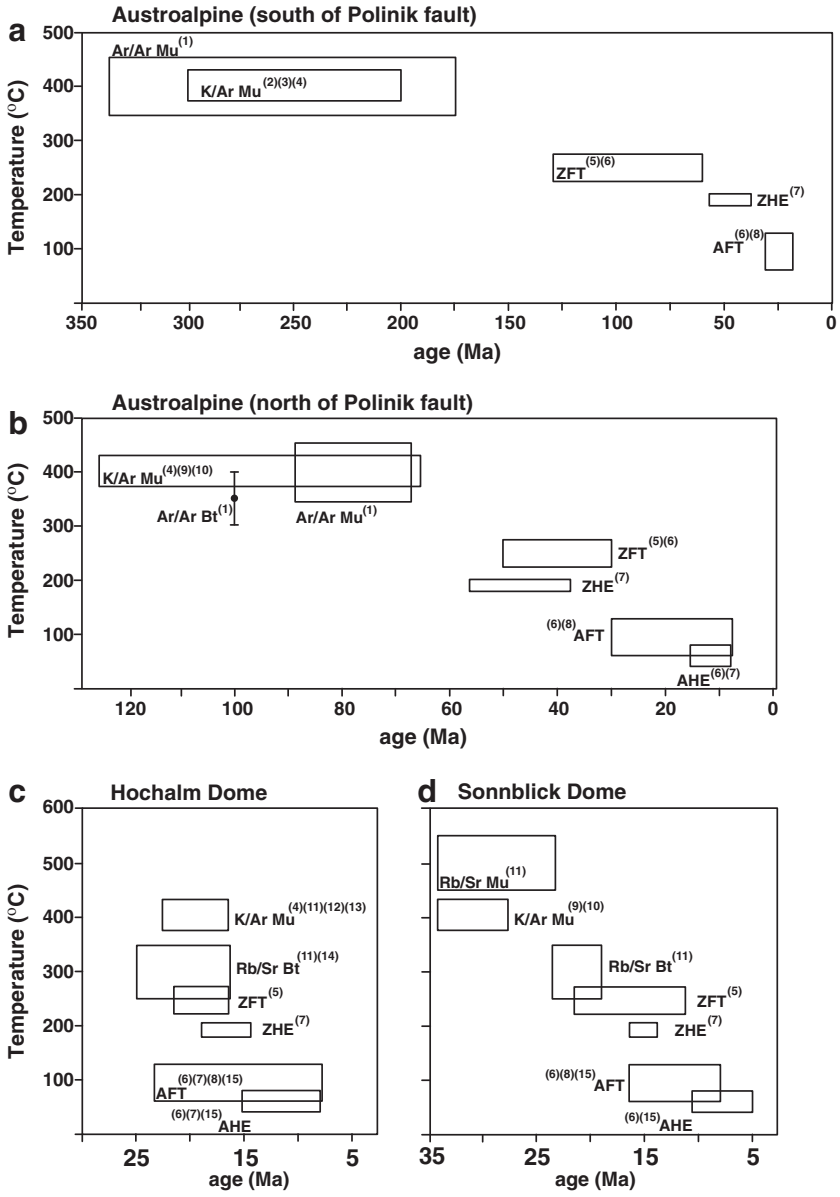

Fig. 4. Available geochronological data from the southeastern Tauern Window and adjacent Austroalpine units. Data are from: (1) Dekant (2009), (2) Brewer and Jenkins (1969), (3) Brewer (1970), (4) Hoke (1990), (5) Dunkl et al. (2003), (6) Wölfler et al. (2008) (7) this study (8) Staufenberg (1987) (9) Lambert (1970), (10) Waters (1976), (11) Reddy et al. (1993), (12) Oxburgh et al. (1966), (13) Cliff et al. (1985), (14) Hawksworth (1976), (15) Foeken et al. (2007); ZFT: Zircon fission track; ZHE: zircon (U–Th)/He; AFT: apatite fission track; AHE: apatite (U–Th)/He; Mu: muscovite; Bt: biotite.

Venediger Nappe, and a Permo-Mesozoic cover, the Glockner Nappe and Matrei Zone (e.g. Frisch, 1980). The Venediger Nappe includes the widely distributed Zentralgneis comprising deformed Variscan granitoids and a parautochtonous cover of Paleozoic metasediments. The Zentralgneis is exposed in a series of domes within the Tauern Window, such as the Zillertal Venediger Domes and the Sonnblick or Hochalm Domes (Fig. 2a). The formation of the dome structures of the Sonnblick and Hochalm Domes occurred shortly after metamorphism (~27 and ~17 Ma, respectively; Kurz and Neubauer, 1996; Reddy et al., 1993).

The study area is situated ~20 km northwest of Lienz (Tyrol/Austria) (Fig. 2a). Here, the Sonnblick and Hochalm Domes as well as the overlying Paleozoic metasediments and the Permo-Mesozoic sequences are of relevance (Fig. 2b). The Sonnblick Dome forms a large northeast-vergent antiformal dome structure that is bordered by the northwest-trending Mallntiz synform (Fig. 2a–c). This synform exposes metasedimentary rocks of the Glockner Nappe. In the study area the Möll valley fault consists of several steep dipping shear zones that cut the Sonnblick Dome at its northeastern border, near the Mallnitz synform (Kurz and Neubauer, 1996) (Fig. 2b). Dextral offset along this part of the Möll valley fault is relatively small and has been estimated to be on the order of ~2.5 km (Kurz and Neubauer, 1996). To the northwest the Sonnblick Dome is bordered by several ductile to brittle normal faults (Fig. 2b). To the south, the Sonnblick Dome is bordered by a sinistral ductile to brittle shear zone, the Moser fault (Fig. 2).

3. Methods

Fission tracks are linear trails of damage in the crystal lattice produced by the spontaneous decay of ^{238}U (Wagner and Van den haute, 1992). We used the apatite fission track method (AFT) with a sensitivity interval between 120 °C and 60 °C (e.g. Gallagher et al., 1998; Green et al., 1986). This temperature range is often referred as apatite partial anealling zone (APAZ) where the fission tracks are progressively shortened, depending on temperature and time

spent in the APAZ. By using fission track length distributions it is therefore possible to investigate the thermal history of the rocks and model the time–temperature trajectory of the sample (e.g. Gleadow et al., 1986a,b; Ketcham, 2005). For more details of the fission track method, the reader is referred to the publication of Wagner and Van den haute (1992).

Spontaneous tracks in apatites were revealed according to the method described by Donelick et al. (1999). We used the external detector method (Gleadow, 1981) with low-uranium muscovite sheets (Goodfellow mica™; Goodfellow GmbH, Badnauheim, Germany). The zeta calibration approach was used (Hurford and Green, 1983) and the FT ages were calculated with the program TRACKKEY version 4.1 (Dunkl, 2002). All track lengths were corrected for c-axis orientation (Donelick et al., 1999). Modeling of the low temperature thermal history based of AFT- and AHE data was carried out using the HeFTy modeling program (Ketcham, 2005) with Dpar values (mean diameters of etch figures on prismatic surfaces of apatites parallel to the crystallographic c-axis) (Burtner et al., 1994). All track lengths were corrected for c-axis orientation (Donelick et al., 1999).

Zircon and apatite (U–Th)/He thermochronology is based on the ingrowth of radiogenic helium produced by the α-decay of U and Th (e.g. Farley, 2002; Reiners et al., 2003). The sensitivity intervals of these thermochronometers are referred to as zircon- and apatite helium partial retention zones (ZHEPRZ, AHEPRZ) with temperature ranges from 200 to 180 °C and 80 to 40 °C (Reiners et al., 2003; Wolf et al., 1996, respectively.

Crystals of apatite and zircon were hand-picked following the selection criteria of Reiners (2005) and Farley (2002), then photographed and measured.

Single crystals of apatite and zircon were loaded in Pt and Nb microtubes, respectively, degassed at ~900 °C (apatite) and ~1200 °C (zircon) under vacuum using laser-heating and analyzed for He using the CSIRO Earth Science and Resource Engineering extraction line in the John de Laeter Centre for Isotope Research in Perth (Australia) on a Pfeiffer Prisma QMS-200 mass spectrometer. The gas extracted minerals were spiked with ^{233}U and ^{230}Th, dissolved and analyzed for U and Th at TSW Analytical Ltd in the University of Western Australia (Perth) on an Agilent 7500 ICP-MS. For more details on analytical procedures, the reader is referred to Danišík et al. (2008) and Evans et al. (2005). The total analytical uncertainty was calculated as a square root of sum of squares of weighted uncertainties on U, Th and He measurements. Replicate analyses of Durango apatite (23 analyses), measured over the period of this study as an internal standard and check of accuracy, yielded a mean age of 30.7 ± 1.0 Ma. This is in good agreement with the Durango AHE age of 31.13 ± 1.01 Ma reported by McDowell et al. (2005).

The raw AHE and ZHE ages were corrected for alpha ejection (Ft) after Farley (2002) and Hourigan et al. (2005), respectively. A value of 5% was adopted as the uncertainty on the Ft correction.

3.1. Sampling strategy

We focused our sampling campaign on a profile that starts from the Austroalpine units (Fig. 2b,c; Fig. 3), from where no AFT, ZHE and AFT ages had been reported. The profile then crossed the Austroalpine/Penninic boundary to the Penninic Sonnblick Dome where it traverses the Möll valley fault within the Penninic units. This transect contains three steep elevation profiles; one in the Austroalpine units and one each to the southeast and northwest of the Möll valley fault (Fig. 3c). The samples span elevations between 1530 and 3015 m above sea level. In order to determine the thermal history of the study area we collected every 200 to 300 m one sample. Unfortunately not all rocks contained enough apatites for fission track- or (U–Th)/He analysis. The samples from the Austroalpine units are garnet micaschists that mainly contain quartz, muscovite and garnets. Those from the Tauern Window are micaschists from the Permo-Mesozoic cover (Glockner Nappe) with muscovite, chlorite, quartz and subordinated calcite and orthogneisses from the Zentralgneis (Fig. 3b, Tables 1, 2, 3). The Zentralgneis consists of coarse grained augen gneisses that are mainly composed of quartz, biotite and feldspar.

3.2. Available thermochronological data

Besides fission track- and apatite (U–Th)/He data, a huge amount of higher temperature thermochronometers that range between ~340 and ~15 Ma are available. These data are $^{40}K/^{39}Ar$ ages of white mica and biotites (Brewer, 1970; Brewer and Jenkins, 1969; Cliff et al., 1985; Hoke, 1990; Lambert, 1970; Oxburgh et al., 1966; Waters, 1976), $^{40}Ar/^{39}Ar$ of white mica and biotites (Dekant, 2009) and $^{87}Rb/^{86}Sr$ data from biotites and white mica (Cliff et al., 1985; Hawkesworth, 1976; Reddy et al., 1993). For the closure temperature ranges of these thermochronometers we follow these authors: $^{40}K/^{39}Ar$ white mica ~430–375 °C (Hames and Bowring, 1994; Kirschner et al., 1996); $^{40}K/^{39}Ar$ biotite ~350–250 °C (Faure and Mensing, 1986); $^{40}Ar/^{39}Ar$ white mica ~450–350 °C (Hames and Bowering, 1994; Harrison et al., 2009; Kirschner et al., 1996; Lips et al., 1998); $^{40}Ar/^{39}Ar$ biotite 400–300 °C (Grove and Harrison, 1996; Villa, 1998); $^{87}Rb/^{86}Sr$ white mica ~550–450 °C (Jäger et al., 1969; Purdy and Jäger, 1976); $^{87}Rb/^{86}Sr$ biotite ~350–250 °C (Del Moro et al., 1982; Jäger et al., 1969). The authors are aware of the fact that the closure temperature concept of distinct thermochronometers is still debated (e.g. Harrison et al., 2009 for diffusion of ^{40}Ar in muscovite). Additionally the large spread of $^{40}K/^{39}Ar$- and $^{40}Ar/^{39}Ar$ ages (Fig. 4a, b) suggest that these ages cannot be considered as "true" cooling ages. If these ages were representing cooling ages they would give a much smaller range. Therefore Fig. 4 should only be considered as a compilation of existing data.

The Austroalpine units to the southeast of the Tauern Window are characterized by different thermochronological ages to the south and north of the Polinik fault, respectively. The southern area is characterized by $^{40}K/^{39}Ar$- and $^{40}Ar/^{39}Ar$ ages of white mica and biotites that range from 337 to 141 Ma (Brewer, 1970; Brewer and Jenkins, 1969; Dekant, 2009; Hoke, 1990; Oxburgh et al., 1966; Waters, 1976) (Fig. 4a). Zircon fission track- (ZFT) and AFT ages are between 160 and 60 (Dunkl et al., 2003; Wölfler et al., 2008) and 30 and 19 Ma (Staufenberg, 1987; Wölfler et al., 2008), respectively (Fig. 4a).

The Austroalpine units to the north of the Polinik fault are part of the Eoalpine high pressure metamorphic belt (e.g. Schuster et al., 2004) and display Cretaceous $^{40}K/^{39}Ar$- and $^{40}Ar/^{39}Ar$ ages of white mica and biotite (Dekant, 2009; Hoke, 1990; Lambert, 1970; Waters, 1976) (Fig. 4b). In this zone ZFT, AFT and AHE ages range from 45 to 30, 19.4 to 7.3, and 16.7 to 10.8 Ma, respectively (Dunkl et al., 2003; Staufenberg, 1987; Wölfler et al., 2008) (Figs. 3a, 4b).

Within the Penninic units of the southeastern Tauern Window the highest temperature thermochronometers are $^{87}Rb/^{86}Sr$ of muscovite, ranging between 34 and 23 Ma (Reddey et al., 1993) (Fig. 4d). Muscovite $^{40}K/^{39}Ar$ ages are between 34.4 and 16.5 Ma (Cliff et al., 1985; Hoke, 1990; Lambert, 1970; Oxburgh et al., 1966; Reddy et al., 1993; Waters, 1976) and document significant earlier cooling of the Sonnblick Dome (34.4–27.5 Ma) than of the Hochalm Dome (22.0–16.5 Ma) (Fig. 4c, d). Biotite $^{40}K/^{39}Ar$ data are only available from the Hochalm Dome, ranging from 22 to 15 Ma (Hoke, 1990). For the Hochalm Dome biotite $^{87}Rb/^{86}Sr$ ages are between 25.4 and 16.5 Ma (Hawkesworth, 1976; Reddy et al., 1993), those from the Sonnblick Dome are from 23.5 to 19.1 Ma (Reddy et al., 1993) (Fig. 4c, d).

ZFT- and AFT ages are 21.5–16.3 Ma (Dunkl et al., 2003) and 21.7–7.8 Ma (Foeken et al., 2007; Staufenberg, 1987; Wölfler et al., 2008), respectively (Fig. 4b, c). AHE ages from the southeastern Tauern Window range between 16.5 and 5 Ma (Foeken et al., 2007; Wölfler et al., 2008) and document earlier cooling of the Hochalm Dome

Table 1
Zircon (U–Th)/He data[a].

Sample code (elevation)	Tectonic unit	Lithology	Longitude	Latitude	Crystal #	Th (ng)	Th error (%)	U (ng)	U error (%)	He (ncc at STP)	He error (%)	TAU (%)	Th/U	Unc. age (Ma)	±1σ (Ma)	F_t	Corr. age (Ma)	±1σ (Ma)
A 47	AuA	micaschist	46°58′53″	12°51′47″	#1	1.526	4.3	1.034	4.3	5.100	0.5	4.3	1.466	30.0	1.3	0.79	38.0	2.5
(1530 m)					#2	0.653	4.4	1.021	4.3	4.024	0.5	4.3	0.636	28.1	1.2	0.77	36.5	2.4
Average age ± standard deviation (in Ma)																	37.3	1.2
A 112	AuA	micaschist	46°58′28″	12°51′20″	#1	0.880	4.3	1.451	4.3	7.522	0.5	4.3	0.602	37.2	1.6	0.79	47.1	1.6
(2000 m)					#2	0.882	4.3	2.984	4.3	12.225	0.5	4.3	0.294	31.4	1.4	0.75	41.9	1.4
					#3	2.332	4.3	2.798	4.3	18.574	0.7	4.3	0.828	45.5	2.0	0.79	57.6	2.0
Average age ± standard deviation (in Ma)																	48.9	8.0
A 42	AuA	micaschist	46°58′07″	12°50′26″	#1	2.508	0.0	6.915	4.2	43.993	0.5	4.2	0.360	48.0	2.0	0.80	60.0	3.9
(2510 m)					#2	2.206	4.3	8.382	4.3	48.830	2.2	4.8	0.261	44.9	2.2	0.76	59.1	4.1
					#3	0.270	4.3	0.660	4.3	2.925	0.6	4.3	0.407	33.2	1.4	0.63	51.1	3.4
Average age ± standard deviation (in Ma)																	56.7	4.9
TW 115	TW	micaschist	47°00′38″	12°52′00″	#1	2.247	4.3	6.302	4.3	9.379	1.8	4.6	0.354	11.3	0.5	0.85	13.3	0.9
(1097 m)	SD				#2	2.083	4.3	5.154	4.3	7.971	1.6	4.6	0.401	11.6	0.5	0.80	14.5	0.9
					#3	1.269	4.3	3.380	4.3	4.847	5.7	7.1	0.373	10.8	0.8	0.79	13.7	0.9
Average age ± standard deviation (in Ma)																	13.8	0.6
TW 114	TW	micaschist	47°00′43″	12°53′40″	#1	0.160	4.4	1.405	4.3	1.923	0.5	4.3	0.113	11.0	0.5	0.82	13.4	0.9
(1653 m)	SD				#2	0.327	4.3	0.970	4.3	1.526	0.5	4.3	0.334	12.0	0.5	0.85	14.1	0.9
					#3	0.738	4.3	2.410	4.4	3.661	0.5	4.4	0.304	11.6	0.5	0.82	14.1	0.9
Average age ± standard deviation (in Ma)																	13.9	0.4
TW 39	TW	micaschist	47°00′44″	12°54′11″	#1	1.032	4.3	2.866	4.3	4.053	3.6	5.6	0.357	10.7	0.6	0.78	13.7	1.0
(2120 m)	SD				#2	1.145	4.3	2.749	4.3	4.371	3.1	5.3	0.414	11.9	0.6	0.80	14.9	1.1
					#3	2.270	4.4	5.803	4.3	8.982	1.2	4.5	0.388	11.6	0.5	0.83	14.0	0.9
Average age ± standard deviation (in Ma)																	14.2	0.6
TW 51	TW	orthogneiss	47°01′33″	12°54′48″	#1	0.652	4.3	1.536	4.3	2.315	0.5	4.3	0.422	11.3	0.5	0.67	16.9	1.1
(2413 m)	SD				#2	1.440	4.3	3.412	4.3	5.056	0.5	4.3	0.419	11.1	0.5	0.78	14.2	0.9
					#3	0.840	4.3	1.897	4.3	2.936	0.5	4.3	0.440	11.5	0.5	0.76	15.1	1.0
Average age ± standard deviation (in Ma)																	15.4	1.4
TW 111	TW	orthogneiss	47°02′29″	12°55′31″	#1	0.354	4.3	0.656	4.3	0.821	1.2	4.5	0.535	9.1	0.4	0.67	13.6	0.9
(2745 m)	SD				#2	0.072	4.3	0.293	4.3	0.396	1.4	4.5	0.244	10.5	0.5	0.65	16.2	1.1
					#3	0.331	4.3	0.738	4.3	1.263	1.2	4.5	0.446	12.7	0.6	0.75	16.9	1.1
Average age ± standard deviation (in Ma)																	15.6	1.7
TW 110	TW	orthogneiss	47°02′49″	12°56′26″	#1	0.735	4.3	1.738	4.3	2.829	0.5	4.3	0.420	12.2	0.5	0.73	16.7	1.1
(2946 m)	SD				#2	0.797	4.3	1.927	4.3	2.868	1.2	4.4	0.411	11.1	0.5	0.71	15.6	1.0
					#3	1.497	4.3	2.709	4.3	4.629	0.5	4.3	0.549	12.4	0.5	0.77	16.1	1.1
Average age ± standard deviation (in Ma)																	16.1	0.6
TW 109	TW	micaschist	47°03′32″	12°59′35″	#1	0.566	4.3	1.540	4.3	2.629	1.2	4.4	0.365	12.9	0.6	0.85	15.2	1.0
(1970 m)	HD				#2	1.239	4.3	1.838	4.3	2.764	0.5	4.3	0.669	10.7	0.5	0.73	14.7	1.0
					#3	0.311	4.3	0.748	4.3	0.956	0.5	4.3	0.413	9.6	0.4	0.70	13.7	0.9
Average age ± standard deviation (in Ma)																	14.5	0.8
TW 105	TW	micaschist	47°03′23″	12°59′08″	#1	0.325	0.0	1.125	4.2	1.956	0.5	4.2	0.286	13.4	0.6	0.85	18.8	1.3
(2220 m)	HD				#2	0.209	0.0	1.465	4.2	2.527	0.5	4.2	0.142	13.7	0.6	0.84	16.3	1.4
					#3	0.106	0.0	0.396	4.2	0.484	0.6	4.2	0.265	9,4	0.4	0.63	14.9	0.8
Average age ± standard deviation (in Ma)																		
TW 108	TW	orthogneiss	47°03′19″	12°58′43″	#1	1.688	4.4	4.074	4.3	6.780	1.2	4.5	0.411	12.5	0.6	0.67	18.7	1.3
(2250 m)	HD				#2	2.272	4.3	4.907	4.3	7.331	5.3	6.8	0.460	11.1	0.8	0.68	16.3	1.4
					#3	0.068	0.0	0.068	4.2	0.089	1.8	4.6	0.991	8.7	0.4	0.70	12.4	0.8
Average age ± standard deviation (in Ma)																	15.8	3.2
TW 44	TW	Orthogneiss	47°02′54″	12°57′13″	#1	0.762	4.3	1.615	4.3	3.551	0.5	4.3	0.468	16.3	0.9	0.85	19.2	1.3
(3015 m)	HD				#2	0.584	4.4	1.775	4.3	3.730	0.5	4.4	0.326	16.0	0.7	0.84	19.0	1.3
Average age ± standard deviation (in Ma)																	19.1	0.1

[a] Th — ^{232}Th; U — amount of ^{238}U and ^{235}U ; He — ^{4}He; TAU — total analytical uncertainty; Unc. age — uncorrected (U–Th)/He age; F_t — alpha recoil correction factor after Hourigan et al. (2005); Cor. age — corrected (U–Th)/He age. AU — Austroalpine; TW — Tauern Window; SD — Sonnblick Dome; HD — Hochalm Dome.

Table 2
Apatite (U–Th)/He data[a].

Sample code (elevation)	Tectonic unit	Lothology	Longitude	Latitude	Crystal #	Th (ng)	Th error (%)	U (ng)	U error (%)	^{4}He (ncc at STP)	^{4}He error (%)	TAU (%)	Th/U	Unc. age (Ma)	±1σ (Ma)	F_t	Corr. age (Ma)	±1σ (Ma)
A 47	AuA	micaschist	46°58′53″	12°51′47″	#1	0.016	0.040	0.018	0.040	0.026	4.6	6.1	0.875	9.5	0.6	0.79	12.0	1.0
(1530 m)					#2	0.087	0.040	0.101	0.040	0.146	2.8	4.8	0.856	9.9	0.5	0.78	12.7	0.9
					#3	0.028	0.040	0.026	0.040	0.046	3.3	5.2	1.086	11.7	0.6	0.79	14.8	1.4
Average age ± standard deviation (in Ma)																	13.2	2.6
A 112	AuA	micaschist	46°58′28″	12°51′20″	#1	0.092	0.040	0.029	0.040	0.056	2.9	4.9	3.104	9.1	0.4	0.68	13.4	0.3
(2000 m)					#2	0.010	0.040	0.025	0.040	0.028	2.8	4.9	0.398	8.4	0.4	0.68	12.4	0.4
					#3	0.064	0.040	0.121	0.040	0.163	2.6	4.7	0.528	9.9	0.4	0.68	14.6	0.4
Average age ± standard deviation (in Ma)																	13.5	1.1
A 42	AuA	micaschist	46°58′07″	12°50′26″	#1	0.058	0.040	0.049	0.040	0.074	2.5	4.6	1.183	9.6	0.4	0.67	14.3	0.7
(2510 m)					#2	1.005	0.040	0.242	0.040	1.016	2.3	4.5	4.129	17.4	0.8	0.73	23.8*	1.2
					#3	0.046	0.040	0.082	0.040	0.143	2.4	4.6	0.562	12.7	0.6	0.79	16.1	0.9
Average age ± standard deviation (in Ma)																	15.2	1.1
A 27	AUA	micaschist	46°58′11″	12°50′35″	#1	0.152	0.040	0.115	0.040	0.315	2.6	4.8	0.198	17.1	0.8	0.75	22.8*	1.6
(2340 m)					#2	0.206	0.040	0.115	0.040	0.109	3.9	5.5	0.299	5.5	0.3	0.77	7.1*	0.5
					#3	0.087	0.040	0.034	0.040	0.200	3.6	5.3	0.292	30.2	1.6	0.68	44.4*	3.2
A 29	AuA	micaschist	46°58′25″	12°51′16″	#1	0.184	0.040	0.109	0.040	0.181	3.9	5.5	1.669	9.7	0.5	0.72	13.5*	1.0
(1840 m)					#2	0.263	0.040	0.057	0.020	0.441	3.1	5.0	4.606	30.5	1.5	0.72	42.6*	3.0
TW 114	TW	micaschist	47°00′43″	12°53′40″	#1	0.230	0.040	0.126	0.040	0.189	3.1	5.0	1.815	8.6	0.4	0.68	12.6*	0.8
(1653 m)	SD				#2	0.230	0.040	0.144	0.040	0.105	3.7	5.3	1.585	4.3	0.2	0.83	5.2	0.4
					#3	0.109	0.040	0.052	0.040	0.030	6.4	7.5	2.071	3.1	0.2	0.83	3.8	0.3
Average age ± standard deviation (in Ma)																	4.5	0.5
TW 39	TW	micaschist	47°00′44″	12°54′11″	#1	0.440	0.020	0.237	0.040	0.196	3.4	5.2	1.846	4.7	0.2	0.85	5.5	0.4
(2120 m)	SD				#2	0.028	0.001	0.040	0.040	0.022	10.9	11.6	0.693	3.9	0.5	0.85	4.6	0.6
Average age ± standard deviation (in Ma)																	5.0	0.6
TW 51	TW	orthogneiss	47°01′33″	12°54′48″	#1	0.161	0.040	0.094	0.040	0.083	2.9	4.9	1.711	5.2	0.3	0.83	6.3	0.4
(2413 m)	SD				#2	0.104	0.040	0.061	0.040	0.052	3.2	5.1	1.691	5.0	0.3	0.85	5.9	0.4
					#3	0.051	0.040	0.052	0.040	0.027	3.1	5.0	0.984	3.4	0.2	0.82	4.1	0.2
Average age ± standard deviation (in Ma)																	5.4	1.2
TW 33	TW	orthogneiss	47°01′56″	12°54′56″	#1	0.197	0.040	0.116	0.040	0.088	1.2	4.1	1.685	4.4	0.2	0.79	5.6	0.4
(2612 m)	SD				#2	0.223	0.040	0.109	0.040	0.077	1.6	4.2	2.029	3.9	0.2	0.80	4.9	0.4
					#3	0.143	0.040	0.082	0.040	0.072	2.0	4.4	1.733	5.1	0.2	0.83	6.1	0.4
Average age ± standard deviation (in Ma)																	5.5	0.6
TW 111	TW	orthogneiss	47°02′29″	12°55′31″	#1	0.190	0.040	0.124	0.040	0.156	1.2	4.1	1.527	7.6	0.3	0.63	12.1*	0.8
(2745 m)	SD				#2	0.103	0.040	0.065	0.040	0.044	3.7	5.4	1.560	4.0	0.2	0.75	5.3	0.4
					#3	0.233	0.040	0.146	0.040	0.112	1.9	4.3	1.583	4.6	0.2	0.75	6.1	0.4
Average age ± standard deviation (in Ma)																		0.6
TW 110	TW	orthogneiss	47°02′49″	12°56′26″	#1	0.398	0.040	0.248	0.040	0.214	1.0	4.0	1.590	5.2	0.2	0.83	6.3	0.2
(2946 m)	SD				#2	0.234	0.040	0.136	0.040	0.131	1.3	4.1	1.707	5.6	0.2	0.85	6.6	0.2
					#3	0.070	0.040	0.035	0.040	0.033	4.2	5.8	1.972	5.2	0.3	0.82	6.3	0.3
Average age ± standard deviation (in Ma)																	6.4	0.2
TW 109	TW	micaschist	47°03′32″	12°59′35″	#1	0.334	0.040	0.161	0.040	0.122	2.4	4.6	2.059	4.2	0.2	0.67	6.3	0.4
(1970 m)	HD				#2	0.228	0.040	0.144	0.040	0.176	2.4	4.6	1.574	7.3	0.3	0.80	9.1	0.6
Average age ± standard deviation (in Ma)																	7.7	2.0
TW 108	TW	orthogneiss	47°03′19″	12°58′43″	#1	0.098	0.040	0.116	0.040	0.077	1.9	4.3	0.844	4.6	0.2	0.63	7.3	0.5
(2250 m)	HD				#2	0.208	0.040	0.145	0.040	0.173	1.9	4.1	1.420	7.3	0.3	0.79	9.2	0.6
					#3	0.078	0.040	0.038	0.040	0.038	4.2	5.8	2.026	5.5	0.3	0.76	7.2	0.6
Average age ± standard deviation (in Ma)																	7.9	1.1
TW 44	TW	orthogneiss	47°02′54″	12°57′13″	#1	0.149	0.040	0.101	0.040	0.325	2.8	4.8	1.460	19.5	0.9	0.70	27.9*	1.9
(3015 m)	HD				#2	0.299	0.040	0.183	0.040	0.182	2.9	4.9	1.618	5.9	0.7	0.65	9.1	0.6
					#3	0.168	0.040	0.071	0.040	0.091	3.1	5.0	2.354	6.8	0.3	0.67	10.1	0.7
Average age ± standard deviation (in Ma)																	9.6	0.7
TW 31	TW	orthogneiss	47°03′00″	12°58′11″	#1	0.125	0.040	0.067	0.040	0.082	4.8	6.2	1.837	7.0	0.4	0.80	8.8*	0.7
(2614 m)	HD				#2	0.095	0.040	0.109	0.040	0.434	2.9	4.9	0.866	27.1	1.3	0.75	36.1*	2.5

[a] Th — ^{232}Th; U — amount of ^{238}U and ^{235}U; He — ^{4}He; TAU — total analytical uncertainty; Unc. age — uncorrected (U–Th)/He age; F_t — alpha recoil correction factor after Farley et al. (1996); Cor. age — corrected (U–Th)/He age. Samples marked by an asterisk were exluded from the calculation of central age and standard deviation and from the interpretation. AU — Austroalpine; TW — Tauern Window; SD — Sonnblick Dome; HD — Hochalm Dome.

Table 3
Apatite fission track data[a].

Sample code	Elevation (m)	Tectonic unit	Lithology	Longitude	Latitude	N	ρ_s	N_s	ρ_i	N_i	ρ_D	Nd	P(χ2) (%)	Age (Ma)	±1σ (Ma)	MTL (μm)	SD (μm)	N(L)	Dpar (μm)
A 47	1530	AuA	micaschist	46°58′53″	12°51′47″	25	0.905	216	4781	1161	4532	11328	98.2	13.8	0.8	14.12	1.01	77	1.85
TW 114	1653	TW (SD)	micaschist	47°00′43″	12°53′40″	25	0.342	88	4377	1082	7756	11328	98.1	7.2	0.5	14.02	0.93	67	1.80
TW 109	1970	TW (HD)	micaschist	47°03′32″	12°59′35″	25	0.507	96	2818	727	5902	11328	99.2	12.8	0.6	13.99	1.14	82	1.92

[a] N — number of dated apatite crystals; ρ_S (ρ_I) — spontaneous (induced) track densities ($\times 10^5$tracks/cm^2); N_s (N_i) — number of counted spontaneous (induced) tracks; ρ_D — dosimeter track density ($\times 10^5$tracks/cm^2); N_d — number of tracks counted on dosimeter; P(χ^2) — probability obtaining Chi-square value (χ^2) for n degree of freedom (where n = no. of crystals − 1); Age ± 1σ — central age ± 1 standard error (Galbraith and Laslett, 1993); MTL — mean track length; SD — standard deviation of track length distribution; N (L) — number of horizontal confined tracks measured; Dpar — average etch pit diameter of fission tracks. Ages were calculated using zeta calibration method (Hurford and Green, 1983), glass dosimeter CN-5, and zeta value of 325.5 ± 1.1 year/cm^2.

(15.2–8.0 Ma) relative to the Sonnblick Dome (10.6–5.0 Ma) (Wölfler et al., 2008) (Fig. 4b, c).

4. Results

The reproducibility of the ZHE ages (n = 37) is good with an average standard deviation of 7.2% (1σ), which is only slightly higher than the analytical uncertainties (Table 1). However, there is significant scatter in the AHE ages with 2 samples revealing single grain ages that are "too old" when compared to corresponding ZHE and/or AFT ages (samples TW 44 and TW 114) (Table 2). Here we follow Lippolt et al. (1994) and suggest that "too old" AHE ages are due to micro-inclusions not detected under 200 fold magnification. In other cases some AHE replicates highly derivate from the mean trend (samples A 42 and TW 111) (Table 2), or cannot be interpreted at all due to their large differences in single grain ages (A 27, A 29, TW 31) (Table 2). These last three samples are therefore not presented in figures and diagrams but are listed in Table 2.

The Austroalpine units yield systematically older ages (ZHE: 56.7–37.3 Ma; AFT: 13.8 Ma, AHE: 15.2–13.2 Ma) than those from the Tauern Window (ZHE: 19.1–13.8; AFT: 12.8 and 7.2 Ma; AHE: 9.6–4.5 Ma) (Figs. 3b, 5a, b, c, Tables 1, 2, 3). The datasets display positive correlation with elevation. Exhumation rates deduced from age-elevation relationships for the Austroalpine samples reveal 0.02 mm/yr ($R^2 = 0.98$) between ~57and 37 Ma for the ZHE system, and 0.4 mm/yr ($R^2 = 0.88$) between ~15 and ~12 Ma for the AHE system (Fig. 5a). However, age-elevation relationships yield numerous uncertainties that will be discussed later. The meant track length of sample A 47 is 14.12 μm indicates rapid cooling through the APAZ (Table 3).

ZHE and AHE ages from the Tauern Window range from 19.1 to 13.8 and 9.6 to 4.5 Ma respectively with a clear trend of younger AFT and AHE ages in the Sonnblick Dome to the south of the Möll valley fault (Figs. 3b, 5b). In the following we refer to the Penninic area to the south of the Möll valley fault as Sonnblick Dome and to the north of it as Hochalm Dome. The AFT ages and mean track length of the Sonnblick- and Hochalm Dome are 7.2 Ma and 14.02 μm and 12.8 Ma and 13.99 μm, respectively (Table 3). The age-elevation relationships deduced from the ZHE system of the Penninic Hochalm and Sonnblick Domes are 0.2 and 0.7 mm/yr, respectively, and therefore

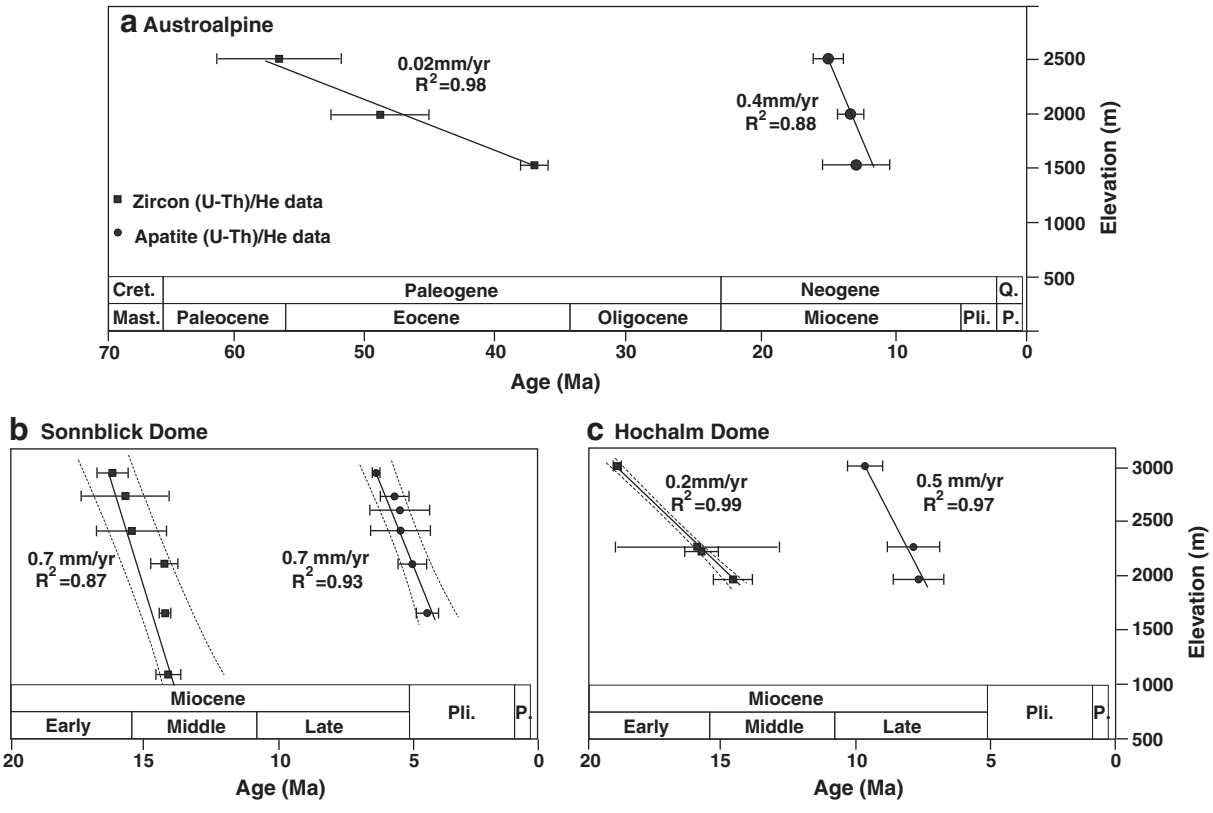

Fig. 5. Age-elevation relationship of the data and apparent exhumation rates derived from them. Exhumation rates (in mm/yr) are calculated as error-weighted linear best fit (solid lines) with 95% confidence level (dashed lines). (a) Austroalpine units and (b) (c) for the Penninic Tauern Window. Cret.: Cretaceous; Mast.: Maastrichtian; Pli.: Pliocene; P.: Pleistocene; Q.: Quaternary.

are different to the north and south of the Möll valley fault (Fig. 5b, c). The AHE system reveals homogeneous exhumation rates to the north and south of fault zone of 0.5 mm/yr. However, to the north of the Möll valley fault exhumation occurred in Late Miocene times, to the south it occurred from Late Miocene to Pliocene times. (Fig. 5b, c).

Based on different closure temperatures of distinct thermochronomters (180 °C for ZHE, 110 °C for AFT and 60 °C for AHE) (Farley, 2000; Gallagher et al., 1998; Reiners et al., 2003; Wolf et al., 1996) our data can also be used to infer cooling histories. These cooling histories are different for the Austroalpine units and the Penninic Hochalm- and Sonnblick Domes (Fig. 6a). The Austroalpine units show very slow cooling rates during the Paleogene and Early Miocene, followed by accelerated cooling in the Middle Miocene at around ~15 Ma (Fig. 6a). Both Penninic domes reveal converse cooling histories. The Hochalm Dome shows rapid cooling in the Middle Miocene around 15 Ma followed by quite low cooling rates after ~12 Ma (Fig. 6a). By contrast, the samples of the Sonnblick Dome record relatively low rates in the Middle Miocene and accelerated cooling in Late Miocene times (Fig. 6a). These similarities and differences between the cooling histories of the Penninic units and Austroalpine are confirmed by a more detailed derivation of the thermal histories using thermal history modeling (Fig. 6b, c, d). The models demonstrate a main phase of cooling in Middle Miocene times (~17 to 12 Ma) for the Austroalpine and the Hochalm Dome (Fig. 6b, c), while the Sonnblick Dome shows later cooling at ~10 to ~7 Ma (Fig. 6d).

5. Discussion

In order to interpret the cooling data presented above in terms of vertical motions in the crust or vertical relative motions across fault zones, a relationship between temperature changes and depth changes must be established. Age-elevation profiles can yield paleo-exhumation rates averaged for the time between the oldest and youngest age of the profile. Thus, different age-elevation trends can, in principle, be used to interpret different exhumation rates. However, this interpretation is subject to potentially large errors if the isotherms at depth are not planar (Stüwe and Hintermüller, 2000; Stüwe et al., 1994). Foeken et al. (2007) have indeed suggested that the warping of isotherms in the southeastern Tauern Window may be substantial enough to influence the interpretation of low temperature thermochronometers. Thus, the interpretation of individual age-elevation profiles in terms of exhumation rates must be treated with caution. Moreover some regressions are defined by only three samples (Fig. 5). Therefore we do not consider the calculated numbers of Fig. 5 as "real" exhumation rates.

However the general trend of increasing exhumation rate for the Austroalpine units equals cooling trends inferred from independent methods. Cooling rates from the mineral pair method suggest an increased cooling for the Austroalpine, a slight increase for the Sonnblick- and a decrease of cooling rate for the Hochalm Dome (Fig. 6a). The mineral pair method does not account for age errors and uncertainties in closure temperatures. Therefore we compare the inferred cooling trends with those from thermal history models that account for these uncertainties and additionally consider track length distribution (Fig. 6b–d).

Interestingly, the general trend of an increasing cooling rate as suggested for the Austroalpine units (Fig. 6a, b) and a decrease in cooling rate during the Middle Miocene for the Hochalm Dome can be established (Fig. 6a,c) However, thermal history models suggest an increase of cooling rate for the Sonnblick Dome during the Late Miocene (Fig. 6d).

These differences may allow us to assess the influence of isothermal warping. For example, Fig. 5 shows that in both the Austroalpine

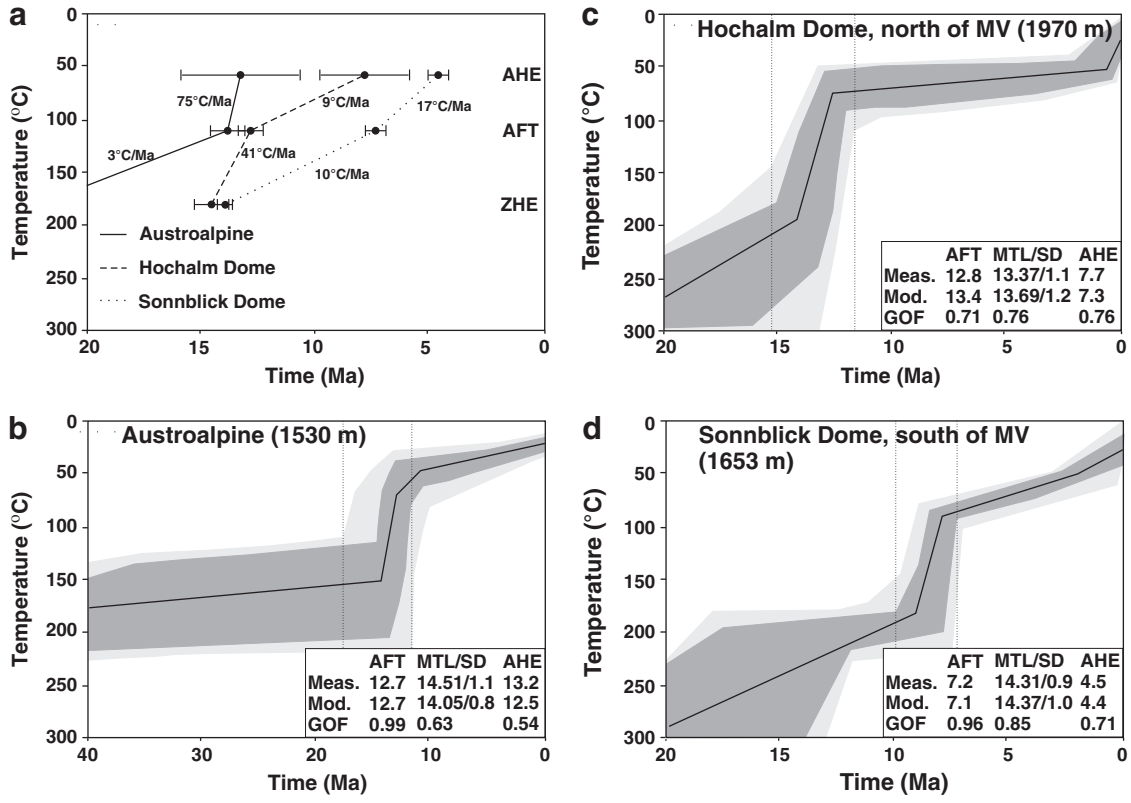

Fig. 6. (a) Cooling rates derived from mineral pairs, black spares and bold line: Austroalpine samples (sample pair A 47), black circles and dashed line: Hochalm Dome (sample pair TW 109); white circles and stippled line: Sonnblick Dome (sample pair TW 114); for the Austroalpine samples only the cooling rate between ZHE- and the AFT system is shown, the ZHE age of 37.3 ± 1.2 Ma is not shown for space reasons. (b–d) Apatite fission track and apatite (U–Th)/He thermal history modeling results using HeFTy (Ketcham, 2005). Input parameters: central AFT age with 1σ error, track length distributions, Dpar values as kinetic parameters. Meas. = measured age; Mod. = modeled age; GOF = goodness of fit.

and the Hochalm Dome, exhumation rates appear to increase with time (i.e. faster apparent exhumation rates at cooler temperatures and later times). This may either be interpreted in terms of (i) more strongly warped isotherms at shallower levels or (ii) increasing exhumation rates or (iii) both (Fig. 7a). As the Austroalpine units and the Hochalm Dome have a similar trend in their age-elevation relationships, but opposing curvature in their cooling histories (Fig. 6a,), this question can be resolved. The cartoon on Fig. 7a illustrates that an increase in apparent exhumation rates on an age-elevation diagram may be caused by warped isotherms, but in that case, will be associated with a decrease in cooling rate on a time-temperature diagram. In contrast, if the increase in apparent exhumation rate on an age-elevation diagram is caused by an increase in exhumation rate, then this will be associated with an increase in cooling rate at lower temperatures. We therefore suggest that the exhumation rate of the Austroalpine did indeed increase from the Paleogene to the Neogene (Fig. 5a) and that the isotherms in the Austroalpine units were not warped. In contrast, we suggest that the exhumation rate in the Hochalm Dome may not have increased with time, but that the isotherms are warped. However, this only applies for the time span between the ZHE- and the AHE partial annealing zone, that is from ~20 to ~7 Ma (between the oldest ZHE- and the youngest AHE age of the Hochalm Dome).

In summary we suggest that age-elevation relationships may lead to false implications about exhumation in the upper crust. Although this has been confirmed in earlier studies (e.g. Stüwe and Hintermüller, 2000; Stüwe et al., 1994) we can use this information to evaluate the connection between warping of isotherms and the formation of topography.

If we consider the perturbation of isotherms in the Hochalm Dome in context with the formation of topography, this interpretation is supported by recent studies. Foeken et al. (2007) demonstrated that the isotherms beneath the southeastern Tauern Window are warped sufficiently to affect at least the 60–40 °C isotherms and the formation of the topography in the Hochalm Dome occurred during Middle- to Late Miocene times. The same applies to Frisch et al. (1998) who reported that relief evolution and formation of topography in the Tauern Window started in the late Middle Miocene and Late Miocene. Although cooling of both, the Penninic- and Austroalpine units, through the APAZ and the HEPRZ occurred during the Middle and Late Miocene (Fig. 6b–d), the Penninic units where always in the position of the footwall (Fig. 7b). Uplift and erosion of the footwall (Tauern Window) as well as the buildup of topography and heat advection can cause significant lateral variations of the Helium closure temperatures (Fig. 7b) (Ehlers and Farley, 2002; Glotzbach et al., 2009). In contrast,isotherms in the hangingwall (Austroalpine)

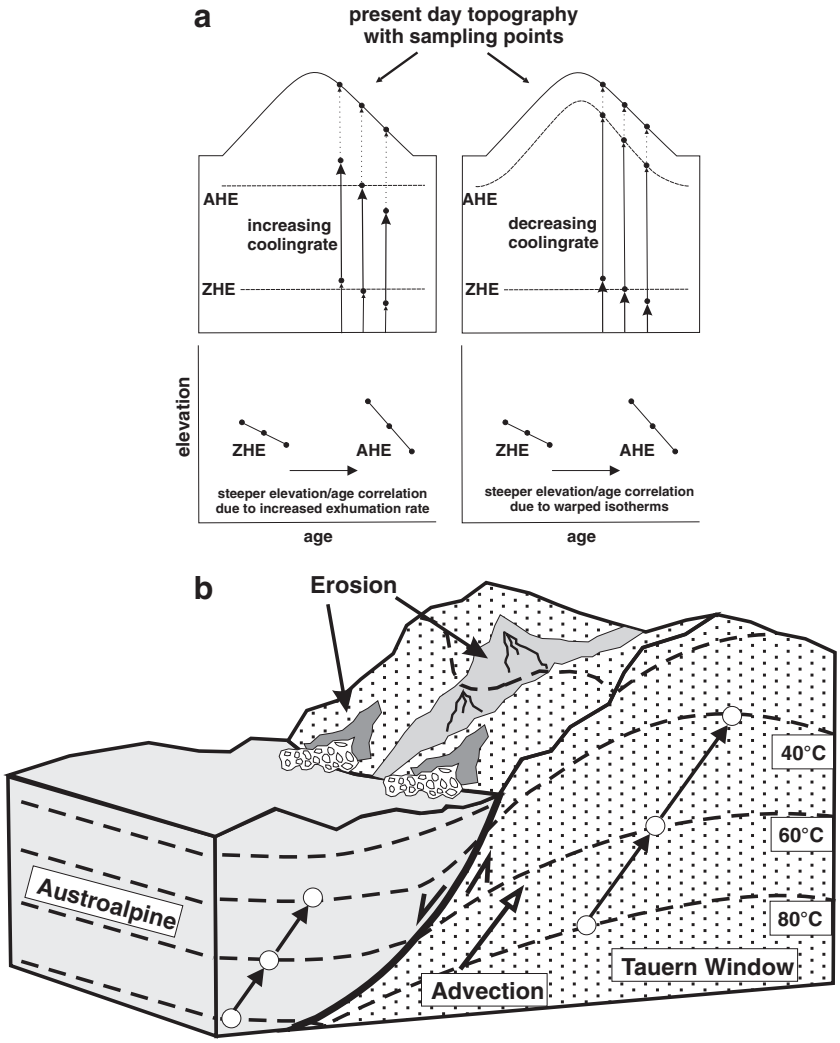

Fig. 7. (a) Relationships between cooling rate and the shape of isotherms: higher cooling rates by planar isothermes and lower cooling rates by warped isotherms (for details see text). (b) Conceptual cartoon illustrating thermal processes that influence the interpretation of low temperature thermochronometers. In the footwall (Tauern Window) isotherms (dashed lines) are curved by topographic relief and/or from advection of mass and heat (see also Ehlers and Farley, 2002; Glotzbach et al., 2009).

are planar or even warped downward due to heat advection (Ehlers and Farley, 2002) (Fig. 7b). Warping of the low temperature isotherms may therefore be expected in similar tectonic settings across the whole European Alps (e.g. Lepontine Dome).

5.1. Exhumation to the southeastern Tauern Window and activity along the Möll valley fault

The generally low exhumation rates of the Austroalpine units during Paleogene times (Fig. 5a) are interpreted to represent the postmetamorphic cooling as observed in different parts of the Eastern Alps (e.g. Dunkl et al., 2003; Hejl, 1997, 1998; Wölfler et al., 2008, 2010). An increase of exhumation rates in the Early to Middle Miocene, as suggested here is quite reasonable and has been demonstrated several times previously (e.g. Fügenschuh et al., 1997; Most, 2003; Staufenberg, 1987; Wölfler et al., 2008). It corresponds to enhanced block movement and exhumation processes in connection with the lateral extrusion in the Eastern Alps.

To infer the relative evolution of tectonic activity in the Hochalm- and Sonnblick Domes, the Austroalpine and the fault zones separating them, we combined the new data with previously published thermochronological ages (Fig. 8). The data suggest different evolution of the Möll valley fault along its northwestern termination within the Tauern Window, where it separates the Sonnblick and Hochalm Domes, and along the part where it separates the Penninic from the Austroalpine units. Therefore we will refer to them as northern and southern Möll valley fault, respectively. As discussed above, the authors are aware of the still ongoing discussion about the closure temperature concept of Ar-dating in white mica (e.g. Harrison et al., 2009). Nevertheless in Fig. 8a we present muscovite $^{40}K/^{39}Ar$ ages for the study area. The different ages between the Penninic Hochalm- (22.0–16.5 Ma) and Sonnblick Dome (34.4–27.5 Ma) might be interpreted as vertical displacement along the northern Möll valley fault (inlay in Fig. 8a). However, due to the difference in $^{40}K/^{39}Ar$ ages vertical displacement must also have taken place along the southern Möll valley fault and along the Penninic/Austroalpine boundary to the south of the Sonnblick Dome (Fig. 8a). Indeed, fault related $^{87}Rb/^{86}Sr$ and $^{40}K/^{39}Ar$ data of the Möll valley fault fall exactly in this time span. These ages range from ~32 to ~22 Ma for the northern Möll valley fault (Cliff and Maffin-Main, 2003; Cliff et al., 1998; Inger and Cliff, 1994) and from ~25 to ~21 Ma for the southern Möll valley fault (Glodny et al., 2008). The wide spread of muscovite $^{40}K/^{39}Ar$ ages in the Austroalpine units to the north (126–66 Ma) and south of the Polinik fault (300–141 Ma) (Fig. 4a, b, Fig. 8a) respectively, cannot be interpreted as cooling ages. Instead they might be ascribed to crystallization ages or inheritance of the crystallization.

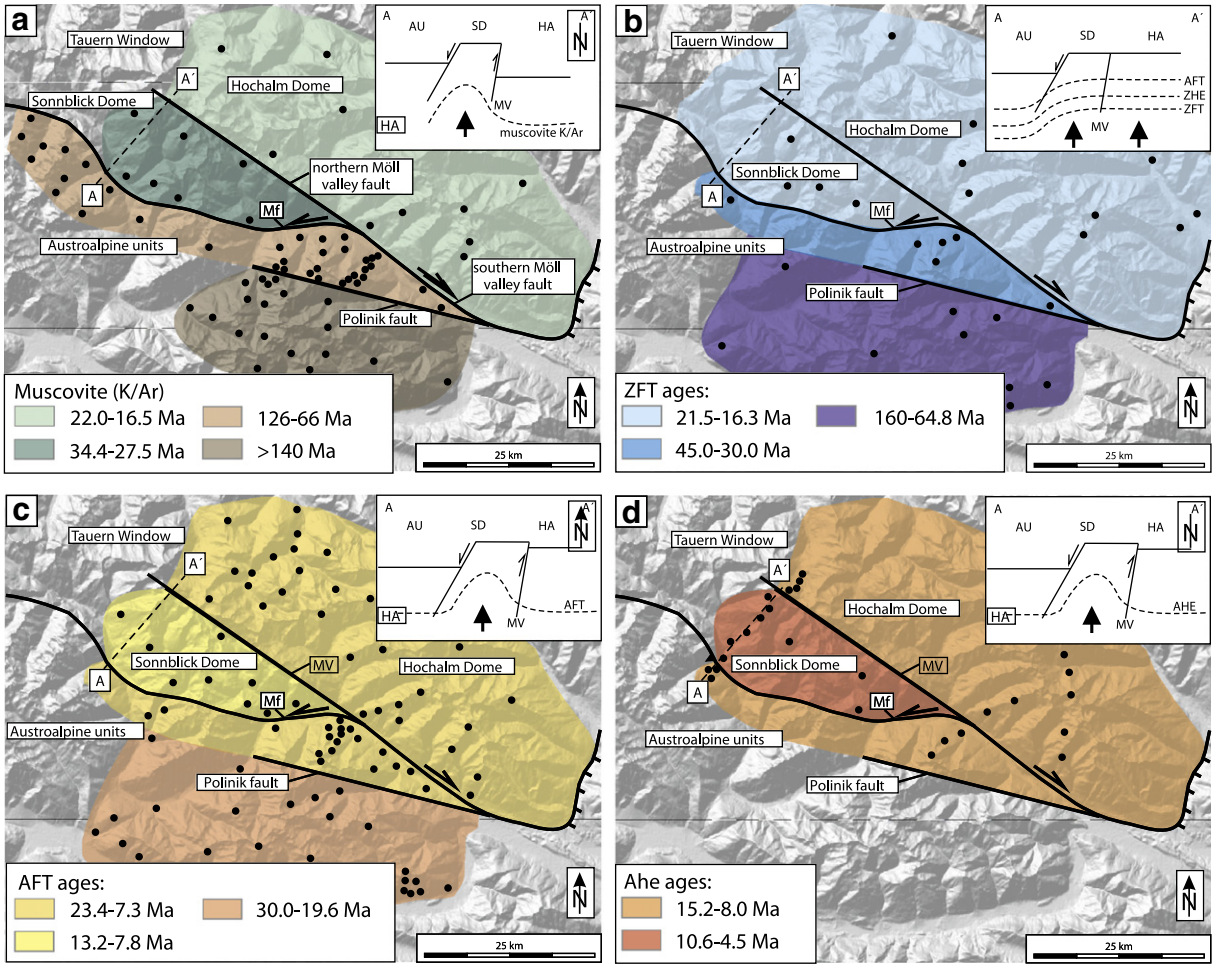

Fig. 8. Summary of geochronological data from the southeastern Tauern Window and adjacent Austroalpine units. For this figure we only used thermochronometers that are available for all four tectonic blocks and that provide a sufficient number of data points to guarantee a well constrained conceptual model. For all other available thermochronometers the reader is referred to Fig. 4 and the main text. Black dots are sample localities. (a) muscovite $^{40}K/^{39}Ar$ ages of the study area; data are from: Hochalm Dome: Oxburgh et al. (1966), Cliff et al. (1985), Hoke (1990), Reddy et al. (1993); Sonnblick Dome: Lambert (1970), Waters (1976), Reddy et al. (1993); between Polinik fault and Tauern Window: Lambert (1970), Waters (1976), Hoke (1990); south of the Polinik fault: Oxburgh et al. (1966), Brewer and Jenkins (1969), Brewer (1970), Waters (1976), Hoke (1990); (b) Zircon fission track ages; data are from: Dunkl et al. (2003), Wölfler et al. (2008); (c) apatite fission track ages; data are from: Staufenberg (1987); Foeken et al. (2007), Wölfler et al. (2008), this study; (d) apatite (U–Th)/He ages; data are from: Foeken et al. (2007), Wölfler et al. (2008), this study.

The available ZFT data show a clear jump to older ages along the Penninic/Austroalpine boundary and along the Polinik fault (Fig. 8b). The homogeneity of these thermochronometers within the eastern Tauern Window does not point to vertical displacement along the northern Möll vally fault, but along the southern Möll valley fault, or rather along the Penninic/Austroalpine boundary (inlay in Fig. 8b). The ZFT ages of the Tauern Window are considered to represent cooling during Early- and Middle Miocene times, thus during the main phase of lateral extrusion and tectonic denudation of the Tauern Window (e.g. Dunkl et al., 2003; Frisch et al., 2000; Wölfler et al., 2008). The Paleogene ZFT and ZHE ages to the southeast of the Tauern Window are considered as postmetamorphic cooling after Eoalpine metamorphism (Figs. 4a, 8b). The Late Jurrasic and Cretaceous ZFT ages to the south of the Polinik fault are consistent with similar ZFT ages of large parts of the Austroalpine units that cooled below the ZFT partial annealing zone before Cenozoic times (Dunkl et al., 2003; Fügenschuh et al., 1997; Hejl, 1997, 1998; Kurz et al., 2011; Luth and Willingshofer, 2008; Wölfler et al., 2008).

A jump in AFT ages does not occur along the Penninic/Austroalpine boundary, but does occur along the Polinik fault (Fig. 8c), which therefore defines the boundary between the tectonically denuded units and the hanging wall at that time (Wölfler et al., 2008). The accumulation of the youngest AFT and AHE ages occurs in the Penninic Sonnblick Dome (Fig. 8c, d), which therefore suggests vertical displacement along the northern Möll valley fault and the southern boundary of the Sonnblick Dome (inlays in Fig. 8c, d), but probably not along the southern Möll valley fault (Wölfler et al., 2008). This is suppurted by thermal history modeling that demonstrates accelerated cooling of the Sonnblick Dome between ~10 and ~7 Ma (Fig. 6d).

In summary we suggest that vertical displacement along the Möll valley fault took place between Oligocene (~34 Ma) and Early Miocene times (~20 Ma). According to the distribution of ZFT ages we conclude that vertical displacement ceased along the northern Möll valley fault, but not along the southern Möll valley fault, where it separates the Penninic- from the Austroalpine units. This is also supported by our thermal history models, that suggest similar cooling trends between ~20 and ~15 Ma for both, the Sonnblick- and Hochalm Dome (Fig. 6c, d). However, horizontal displacement during this time frame, as reported by Frisch et al. (2000) cannot be excluded by our data. During the Middle- and Late Miocene vertical displacement can be observed along the northern Möll valley fault, but probably not along the southern Möll valley fault. This is supported by the distribution of AFT- and apatite (U–Th)/He ages, by thermal history modeling and by previous studies (Wölfler et al., 2008).

5.2. Temporal and geometrical relationship of fault zones in the eastern part of the Tauern Window and implications for the extrusion of the European Alps

The data from this study and previously published work (Dunkl et al., 2003; Foeken et al., 2007; Reinecker, 2000; Staufenberg, 1987; Wölfler et al., 2008, 2011) can be combined to place temporal constraints on the genesis of complex structures that define the extruding block to the east of the Tauern Window (Fig. 9), i.e.in the Katschberg-, Polinik-, Möll valley and along the Mur–Mürz faults. During the main phase of lateral extrusion, (i.e. between ~23 and 12 Ma; Frisch et al., 2000), vertical displacement of the Hochalm Dome and a sliver of Austroalpine units to the north of the Polinik fault were compensated for by normal faulting along the Katschberg- and Polinik faults. Normal fault displacement of both the Katschberg- and Polinik faults were transferred into the Möll valley fault (Frisch et al., 2000; Kurz and Neubauer, 1996; Wölfler et al., 2008). A similar scenario has been proposed for the Mur–Mürz fault system where Reinecker (2000) demonstrated normal faulting of the Gurktal Block (Fig. 9) contemporaneous to activity of the Katschberg normal fault, exhumation of the Niedere Tauern and sedimentation in intramontane

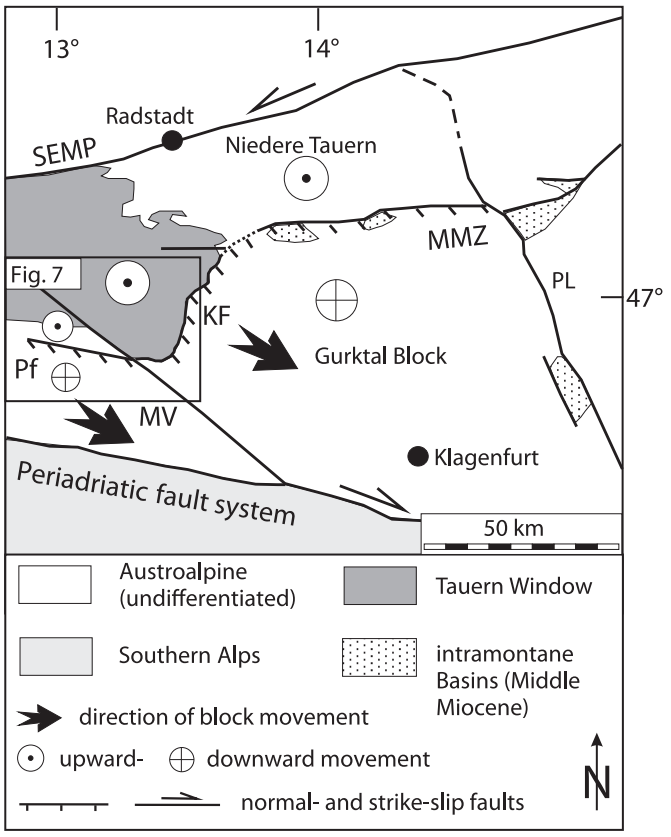

Fig. 9. Sketch map of the Eastern Alps between the eastern Tauern Window and Pöls–Lavanttal fault system. The figure demonstrates fault activity and exhumation of distinct crustal blocks during Miocene lateral extrusion. Southeastward detachment of the Gurktalblock and the Austroalpine units to the south of the Polinik fault occurred during coeval exhumation of the eastern Tauern Window, the Austroalpine units to the north of the Polinik fault and the Niedere Tauern (see also Wölfler et al., 2011). Big black arrows showing the movement direction of crustal blocks to the south and east of the Tauern Window; Pf: Polinik fault; MV: Möll valley fault; SEMP: Salzach–Ennstal–Mariazell Puchberg fault system; MMZ: Mur–Mürz fault system; PL: Pöls–Lavanttal fault system KF: Katschberg normal fault.

basins to the east of the Tauern Window (Wölfler et al., 2011). In summary we suggest that a main phase of fault activity occurred during Middle Miocene times. Time constraints are provided by depositional ages within pull apart basins along strike slip faults (Fig. 9) and by Middle Miocene radiometric ages from shear zones in and around the Tauern Window (Glodny et al., 2008; Wölfler et al., 2011 and references therein).

Generally, geochronological data of fault zones in the Eastern Alps are very rare. However, Glodny et al. (2008) drew two peaks of deformation ages, one in the Oligocene between 32 and 30 Ma and the second in the Early to Middle Miocene between 21 and 15 Ma.

During the Oligocene normal faulting along the Katschberg- and Brenner- normal faults, is documented by numerous geochronological data (Glodny et al., 2008 and references therein). Direct dating of fault activity revealed ~22 Ma and ~21 to 18 Ma for the Katschberg- and Brenner normal faults, respectively (Glodny et al., 2008; Liu et al., 2001). These Early to Middle Miocene deformational ages are in the same range than ZFT cooling ages from the footwall (Fig. 10), demonstrating contemporaneous exhumation and deformation.

Interestingly, similar time ranges for deformation are known from the Western- and Central Alps. Here, ductile mid-crustal deformation is evidenced by mylonites formed in a right-lateral kinematic setting (Fig. 10). These motions are dated at 26–20 Ma in the Argentera-Mercantour Massif (Sanchez et al., 2011), at 20–16 Ma in the Mont Blanc area (Rolland et al., 2007, 2008) and 20–12 Ma in the Aar Massif (Challandes et al., 2008; Rolland et al., 2009a,b) (Fig. 10). Again, ZFT

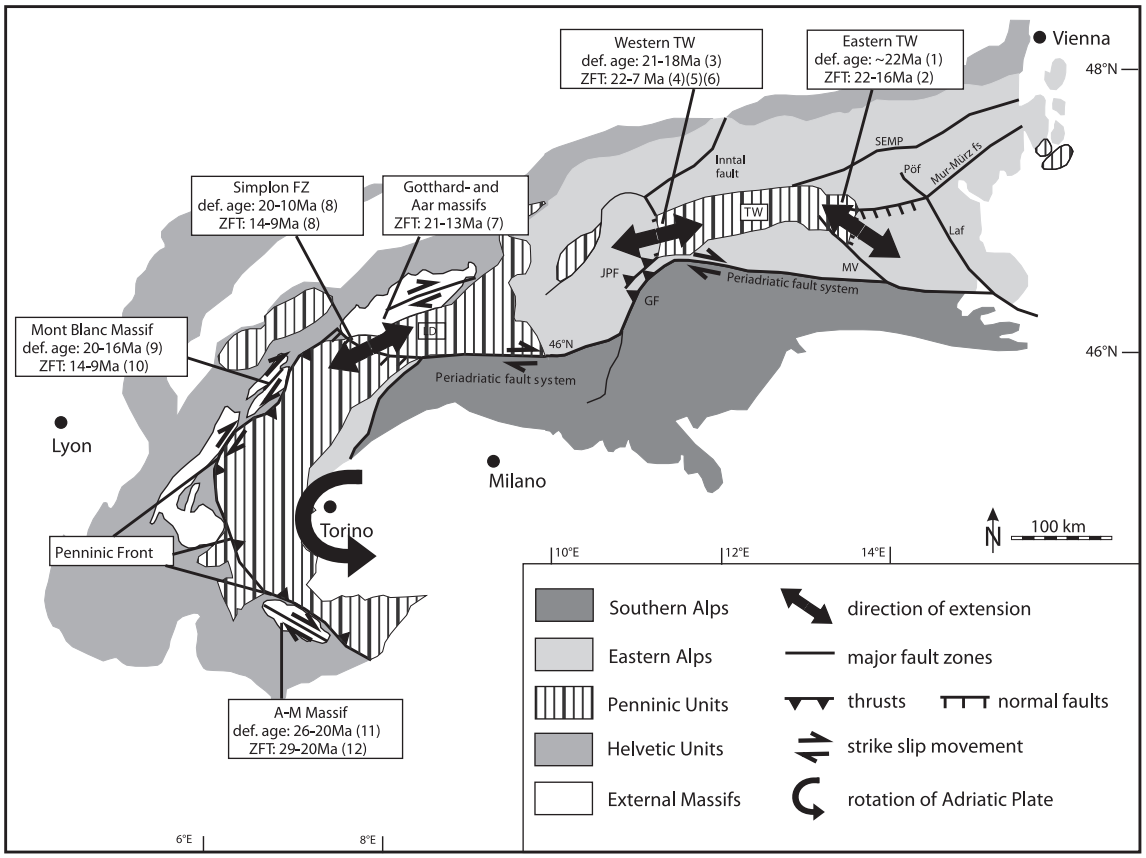

Fig. 10. Fault related data ($^{87}Rb/^{86}Sr$-, $^{40}K/^{39}Ar$- ages) of extensional shear- and strike slip faults in the European Alps. These deformational ages are similar to ZFT cooling ages of the corresponding footwall. TW: Tauern Window, GF: Giudicarie fault; JPF: Jaufen–Passeier fault LD: Lepontine Dome, Simplon FZ: Simplon fault zone, A–M Massif: Argentera–Mercantour Massif. (1) Liu et al. (2001), (2) Dunkl et al. (2003), (3) Glodny et al. (2008), (4) Fügenschuh (1995), (5) Fügenschuh et al. (1997), (6) Most (2003), (7) Glotzbach et al. (2010), (8) Campani et al. (2010), (9) Rolland et al. (2008), (10) Glotzbach et al. (2011b), (11) Sanchez et al. (2011), (12) Bigot-Cormier et al. (2006).

cooling ages are equal to deformation (Fig. 10). As pointed out by Schmid et al. (1989) and Frisch et al. (2000), normal faulting along the Simplon fault zone and contemporaneous exhumation of the Lepontine Dome (Fig. 10), as well as the activity along the Brenner- and Katschberg normal faults are triggered by the NW-indentation of the Adriatic plate. However such indentation would have resulted in sinistral shear in the Western- and Central Alps (Rolland et al., 2012). But it produced dextral shearing along the Penninic Front from the Central Alps to the Argentera–Mercantour Massif (Fig. 10). Therefore Rolland et al. (2012) suggested an alternative model where anticlockwise rotation of the Adriatic plate triggered the overall dextral shear as well as extension perpendicular to the strike of the orogen (Fig. 10).

Counterclockwise rotation of the Adriatic plate started in Oligocene times (Collombet et al., 2002). This is supported by geochronological data that suggest a change from sinistral to dextral kinematics along the Periadriatic fault system (Mancktelow et al., 2001; Müller et al., 2000).

However, extrusion related deformation in the Eastern Alps is not only forced by indentation and/or rotation of the Adriatic plate. In the Eastern Alps an eastward retreating subduction zone in the Carpathians provided the space for material flow to the east (Ratschbacher et al., 1991a). Wölfler et al. (2011) suggested that since Middle Miocene times (~15 Ma), extrusion related faulting to the east of the Katschberg normal fault is much more related to the retreating subduction zone in the Carpathians than to rotation and/or indentation of the Adriatic plate. In addition to Rolland et al. (2012) we suggest that both, rotation of the Adriatic plate and subduction in the Carpathians played a key role in the Miocene extrusion of the European Alps.

5.3. Implications for topographic evolution

There is an ongoing discussion about the cause of the apparent increase in sedimentation rate during the Miocene and Pliocene (Glotzbach et al., 2011a; Schumer and Jerolmak, 2009; Willenbring and von Blanckenburg, 2010; Willett, 2010) and its relationship to the age of topography of the Alps (Hergarten et al., 2010). In order to contribute to this discussion, we compare our data with previously published rates of sediment production from the Alps (Kuhlemann, 2000; Willett, 2010) (Fig. 11).

There is a dramatic increase in sediment discharge rates between 18 and 16 Ma that coincides with the ZFT and ZHE data from the eastern Tauern Window (Fig. 11a). This temporary rise of sediment flux is correlated with the axial updoming of core complexes like the Tauern Window, or the Lepontine Dome in the Central Alps (Fig. 10) (Kuhlemann, 2007). However, ZFT cooling ages of the Lepontine dome record a younger exhumation pulse (~14–9 Ma) (Glotzbach et al., 2011b) than in the eastern Tauern Window (22–16 Ma) (Dunkl et al., 2003) (Fig. 10). On the other hand, $^{40}Ar/^{39}Ar$ detrital ages of white mica demonstrate exposure of the Lepontine Dome between ~20 and 15 Ma (von Eynatten et al., 1999). We suggest that the Middle Miocene exhumation pulse documented by the ZFT and ZHe age pattern presented here relates to a pulse in surface uplift rate that ultimately results in the increased sedimentation rates. Alternatively, the exhumation documented by our data would have been caused predominantly by lateral extension without the requirement of surface uplift and erosion. In that case no correlation of exhumation and sediment discharge would have been expected.

After about 15 Ma, there is no clear correlation between the inferred accelerated sediment accumulation and the AFT or AHE age

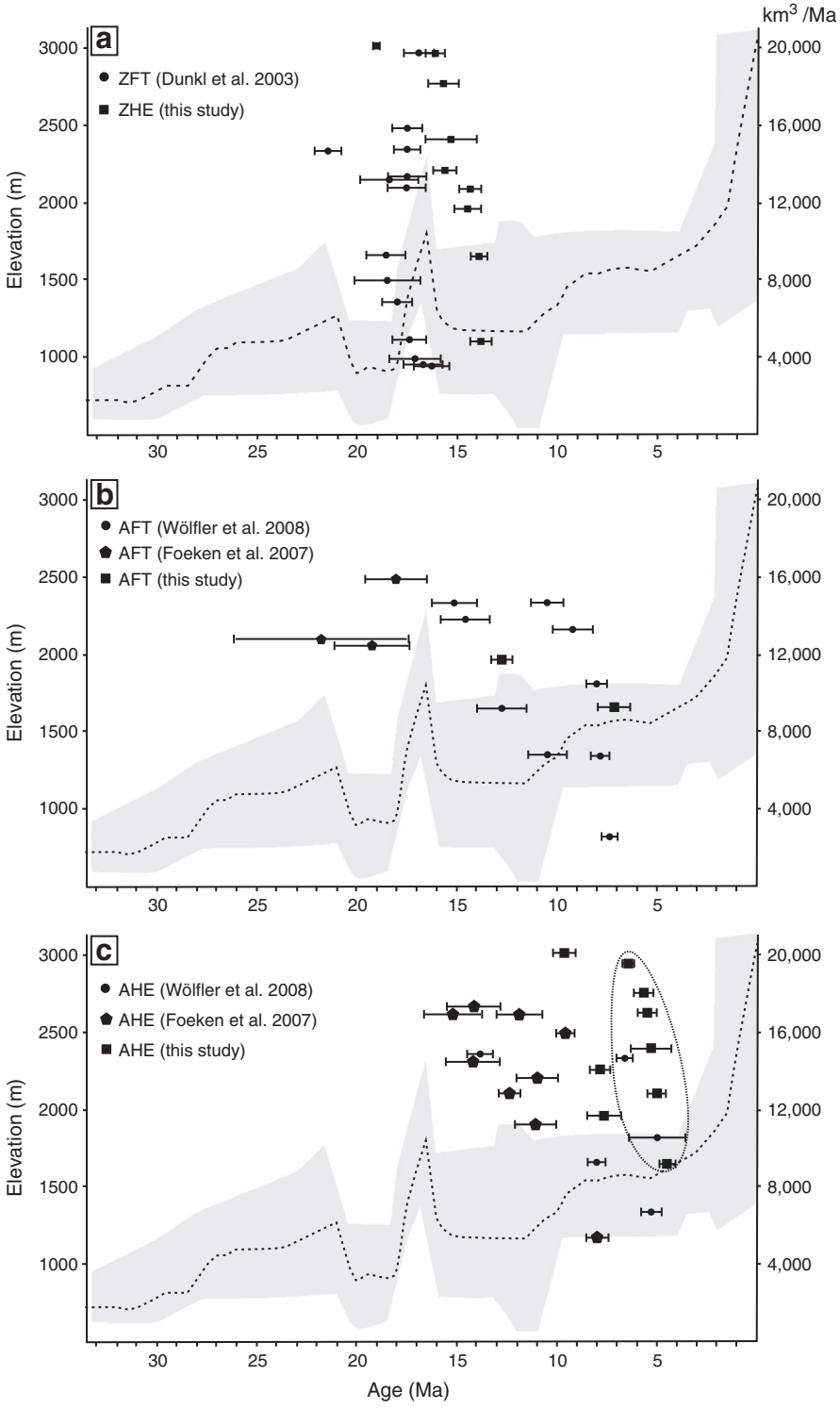

Fig. 11. Comparison of low temperature thermochronological ages of the southeastern Tauern Window with sediment budget of the Alps of Kuhlemann et al. (2002). Data are from: Dunkl et al., 2003; Foeken et al. (2007), Wölfler et al. (2008) and this study. Looped AHE ages are from the Sonnblick Dome.

pattern presented here (Fig. 11b, c). AHE ages of the Sonnblick Dome (Fig. 11c within the loop) are generally somewhat younger than those from the Hochalm Dome but neither corresponds to times of enhanced sediment discharge. The most significant erosion event in this time — the rise of sediment discharge in the last 4–5 My (Kuhlemann, 2000), is not established by our data.

In summary we suggest that fission track data of the Eastern Alps show a good correlation with increased sediment flux in the Middle Miocene (18–16 Ma), but do not correlate with accelerated sediment production at Late Miocene/Early Pliocene times. The average erosion rate of the eastern part of the Eastern Alps is estimated around 0.04 km/My, in line with AFT ages (Hejl, 1997; Wölfler et al., 2010). This very low erosion rate is consistent with the preservation of pre-extrusion paleosurfaces (Frisch et al., 2000) to the east of the Tauern Window. This strongly contradicts a climate trigger for surface uplift in the Eastern Alps, and probably for the whole European

Alps. Instead a tectonic trigger and/or deep-seated mechanism are probably more obvious models to explain surface uplift in the Alps (e.g. Genser et al., 2007).

6. Conclusions

New zircon (U–Th)/He, apatite fission track and apatite (U–Th)/He data from a profile crossing the Austroalpine/Penninic boundary as well as the Möll valley fault south east of the Tauern Window provides new constraints on exhumation, faulting history and topographic evolution in the eastern part of the Eastern Alps. The most important results are summarized as follows:

- Ages from the Austroalpine units revealed by all thermochronometers are systematically older than those from the Tauern Window.
- Age-elevation relationships may lead to false implications about exhumation and cooling in the upper crust.
- Exhumation rates in the Penninic footwall did not increase during the Middle Miocene and low temperature isotherms are warped sufficiently to affect at least the apatite (U–Th)/He ages. Warping of the isotherms is explained by footwall uplift, erosion and the evolution of topography.
- In contrast, exhumation rates of the Austroalpine hangingwall units increased from the Paleogene to the Neogene and the isotherms in this unit are not warped.
- The new data document a Middle Miocene exhumation pulse that is correlated with footwall uplift of Penninic units that can be observed contemporaneous in the Eastern- Western- and Central Alps.
- Fission track- and (U–Th)/He thermochronometers do not record enhanced exhumation- and sedimentation rates in the Eastern Alps. This is in contradiction to models that propose a climatic trigger for surface uplift in the Alps.
- Geochronological ages demonstrate Oligocene to Late Miocene fault activity along the Möll valley fault that plays a crucial role during Middle Miocene lateral extrusion.
- Together with the Katschberg normal fault, the Polinik- and Mur–Mürz fault, the Möll valley fault defines the extruding wedge in the eastern part of the Eastern Alps.
- During the Middle Miocene, enhanced fault activity contemporaneous to footwall cooling (Tauern Window, Lepontine Dome) can be observed in the Alps. This may be related to anticlockwise rotation of the Adriatic plate that forms a shear belt that triggered dextral shear as well as extension perpendicular to the strike of the orogen.

Acknowledgments

This study was carried out within the research projects I152 TOPO-ALPS and I152-N19, granted by the European Science Foundation (ESF) and the Austrian Science Fund (FWF), respectively. Anke Wölfler is thanked for her help with some statistical problems. The constructive reviews of Pierre Valla and Yann Rolland led to a substantial improvement of the manuscript.

References

Bigot-Cormier, F., Sosson, M., Poupeau, G., Stephan, J.-F., Labrin, E., 2006. The denudation history of the Argentera Alpine External Crystalline Massif (Western Alps, France-Italy): an overview from the analysis of fission tracks in apatites and zircons. Geodinamica Acta 19 (6), 455–473.

Bogandoff, S.A., Michard, M., Mansour, M., Poupeau, G., 2000. Apatite fission track analysis in the Argentera massif: evidence of contrasting denudation rates in the external crystalline massifs of the western Alps. Terra Nova 12, 117–125. doi:10.1046/j.1365-3121.2000.00281.x.

Brewer, M., 1970. K-Ar age studies in the Eastern Alps – the Oberostalpindecke of Kärnten. Unpublished PhD Thesis, University of Oxford.

Brewer, M., Jenkins, H., 1969. Excess radiogenic argon in metamorphic micas from the Eastern Alps, Austria. Earth and Planetary Science Letters 6, 321–331.

Burg, J.P., Sokoutis, D., Bonini, M., 2002. Model-inspired interpretation of seismic structures in the Central Alps: wedging and buckling at mature of collision. Geology 30, 643–646.

Burtner, R.L., Nigrini, A., Donelick, R.A., 1994. Thermochronology of Lower Cretaceous source rocks in the Idaho–Wyoming thrust belt. AAPG Bulletin 78, 1613–1636.

Campani, M., Mancktelow, N., Seward, D., Rolland, Y., Müller, W., Guerra, I., 2010. Geochronological evidence for continuous exhumation through the ductile–brittle transition along a crustal-scale low-angle normal fault: Simplon Fault Zone, central Alps. Tectonics 29, TC3002. doi:10.1029/2009TC002582.

Cederbom, C.E., Sinclair, H.D., Schlunegger, F., Rahn, M., 2004. Climate-induced rebound and exhumation of the European Alps. Geology 32, 709–712.

Cederbom, C.E., van der Beek, P., Schlunegger, F., Sinclair, H.D., Oncken, O., 2011. Rapid extensive erosion of the North Alpine foreland basin at 5–4 Ma. Basin Research 23, 528–550. doi:10.1111/j.1365-2117.2011.00501.x.

Challandes, N., Marquer, D., Villa, I.M., 2008. P–T–t modelling, fluid circulation, and ^{39}Ar–^{40}Ar and Rb–Sr mica ages in the Aar Massif shear zones (Swiss Alps). Swiss Journal of Geosciences 101, 269–288.

Cliff, R.A., Meffan – Main, S., 2003. Evidence from Rb–Sr microsampling geochronology for the timing of Alpine deformation in the Sonnblick Dome, SE Tauern Window. In: Vance, D., Müller, W., Villa, I.M. (Eds.), Geochronology: Linking the Isotopic Record with Petrology and Textures: Geol. Soc. Spec. Publ., 220, pp. 159–172.

Cliff, R.A., Droop, G.T.R., Rex, D.C., 1985. Alpine metamorphism in the south-east Tauern Window, Austria: II heating, cooling and uplift rates. Journal of Metamorphic Geology 3, 403–415.

Cliff, R.A., Oberli, F., Meier, M., Droop, G.T.R., 1998. Achieving geological precision in metamorphic geochronology: a Th–Pb age for the syn-metamorphic formation of the Mallnitzermulde synform, Tauern Window, from individual allanite porphyroblasts. Mineralogical Magazine 62A, 337–338.

Collombet, M., Thomas, J.-C., Chauvin, A., Tricart, P., Bouillin, J.-P., Gratier, J.-P., 2002. Counterclockwise rotation of the Western Alps since the Oligocene: new insights from paleomagnetic data. Tectonics 21, 14–21.

Danišík, M., Sachsenhofer, R.F., Privalov, V.A., Panova, E.A., Frisch, W., Spiegel, C., 2008. Low-temperature thermal evolution of the Azov Massif (Ukrainian Shield–Ukraine) — implications for interpreting (U–Th)/He and fission track ages from cratons. Tectonophysics 456, 171–179.

Decker, K., Peresson, H., 1996. Tertiary kinematics in the Alpine–Carpathian–Pannonian system: links between thrusting, transform faulting and crustal extension. In: Wessely, G., Liebl, W. (Eds.), Oil and gas in alpidic thrustbelts and basins of Central and Eastern Europe: EAGE Spec. Publ., 5, pp. 69–77.

Dekant, C., 2009. Investigations on the magmatic and metamorphic history of the Kreuzeck Massif, Carinthia, Austria. Tübinger Geowissenschaftliche Arbeiten Reihe A 75 68 pp.

Del Moro, A., Puxeddu, M., Radicatie De Brozolo, F., Villa, I.M., 1982. Rb–Sr and K–Ar ages on minerals at temperatures of 300–400 °C from deep wells in de Larderello geothermal field (Italy). Contributions to Mineralogy and Petrology 81, 340–349.

Donelick, R.A., Ketcham, R.A., Carlson, W.D., 1999. Variability of apatite fission track annealing kinetics II: crystallographic orientation effects. American Mineralogist 84, 1224–1234.

Dunkl, I., 2002. TRAKKEY: a windows program for calculation and graphical presentation of fission track data. Computers & Geosciences 2, 3–12.

Dunkl, I., Frisch, W., Grundmann, G., 2003. Zircon fission track thermochronology of the southeastern part of the Tauern Window and the adjacent Austroalpine margin, Eastern Alps. Eclogae Geologicae Helvetiae 96, 209–217.

Dunkl, I., Kuhlemann, J., Reinecker, J., Frisch, W., 2005. Cenozoic relief evolution of the Eastern Alps — constraints from apatite fission track age-provenance of neogene intramontane sediments. Australian Journal of Earth Sciences 98, 92–105.

Ehlers, T.S., Farley, K., 2002. Apatite (U–Th)/He thermochronometry: methods and applications to problems in tectonic and surface processes. Earth and Planetary Science Letters 206, 1–13.

Evans, N.J., Byrne, J.P., Keegan, J.T., Dotter, L.E., 2005. Determination of uranium and thorium in zircon, apatite and fluorite: application to laser (U–Th)/He thermochronology. Journal of Analyical Chemistry 60, 1159–1165.

Farley, K., 2000. Helium diffusion from apatite: general behavior as illustrated by Durango fluorapatite. Journal of Geophysical Research 105, 2903–2914.

Farley, K., 2002. (H–Th)/He dating: techniques, calibrations and applications. Mineralogical Society of America. Reviews in Mineralogy & Geochemistry 47, 819–844.

Farley, K.A., Wolf, R.A., Silver, L.T., 1996. The effect of long alpha-stopping distances on (U-Th)/He 486 ages. Geochim. Cosmochim. Acta 60 (21), 4223–4229.

Faure, G., Mensing, T.M., 1986. Isotopes. Principles and Applications. John Wiley & Sons, Inc. 897 pp.

Foeken, J.P.T., Persano, C., Stuart, F.M., Voorde, T.M., 2007. Role of topography in isotherm perturbation: apatite (U–Th)/He and fission track results from the Malta Tunnel, Tauern Window, Austria. Tectonics 26, TC3006. doi:10.1029/2006TC002049.

Frisch, W., 1980. Post-Hercynian formations of the western Tauern window: sedimentological features, depositional environment and age. Mitteilungen der Österreichischen Goelogischen Gesellschaft 71/72, 49–63.

Frisch, W., Kuhleman, J., Dunkl, I., Brügl, A., 1998. Palinspastic reconstruction and topographic evolution of the Eastern Alps during late Tertiary tectonic extrusion. Tectonophysics 297, 1–15.

Frisch, W., Dunkl, I., Kuhlemann, J., 2000. Post-collisional orogen-parallel large-scale extension in the Eastern Alps. Tectonophysics 327, 239–265.

Fügenschuh, B., 1995. Thermal and kinematic history of the Brenner area. ETH Zürich, Swiss, unpubl. Ph.D., 225 pp.

Fügenschuh, B., Seward, D., Mancktelow, N., 1997. Exhumation in a convergent orogen: the western Tauern Window. Terra Nova 9, 213–217.

Galbraith, R.F., Laslett, G.M., 1993. Statistical models for mixed fission track ages. Nucl. Tracks Radiat. Meas. 21, 459–470.
Gallagher, K., Brown, R., Johnson, C., 1998. Fission track analysis and its applications to geological problems. Annual Review of Earth and Planetary Sciences 26, 519–572.
Genser, J., Neubauer, F., 1989. Low angle normal faults at the eastern margin of the Tauern window (Eastern Alps). Mitteilungen der Österreichischen Goelogischen Gesellschaft 81, 233–243.
Genser, J., Cloething, S.A.P.L., Neubauer, F., 2007. Late orogenic rebound and oblique Alpine convergence: new constraints from subsidence analysis of the Austrian Molasse basin. Global and Planetary Change 58, 214–233.
Gleadow, A.J.W., 1981. Fission-track dating methods: what are the real alternatives? Nuclear Tracks 5, 3–14.
Gleadow, A.J.W., Duddy, I.R., Green, P.F., 1986a. Fission track lengths in the apatite annealing zone and the interpretation of mixed ages. Earth and Planetary Science Letters 78, 245–254.
Gleadow, A.J.W., Duddy, I.R., Green, P.F., 1986b. Confined fission track lengths in apatite. A diagnostic tool for thermal history analysis. Contributions to Mineralogy and Petrology 94, 405–415.
Glodny, J., Ring, U., Kühn, A., 2008. Coeval high-pressure metamorphism, thrusting, strike-slip and extensional shearing in the Tauern Window, Eastern Alps. Tectonics 27, TC4004. doi:10.1029/2007TC002193.
Glotzbach, C., Reinecker, J., Danišík, M., Rahn, M., Frisch, W., Spiegel, C., 2008. Neogene exhumation history of the Mont Blanc massif, western Alps. Tectonics 27, TC4011. doi:10.1029/2008TC002257.
Glotzbach, C., Spiegel, C., Reinecker, J., Rahn, M.K., Frisch, W., 2009. What perturbs isotherms? An assessment using fission track thermochronology and thermal modelling along the Gotthard transect, central Alps. In: Lisker, et al. (Ed.), Thermochronological methods: from paleotemperature constraints to landscape evolution models: Geol. Soc. Spec. Publ., 324, pp. 111–124.
Glotzbach, C., Reinecker, J., Danišík, M., Rahn, M., Frisch, W., Spiegel, C., 2010. Thermal history of the central Gotthard and Aar massifs, European Alps: evidence for steady state, long-term exhumation. Journal of Geophysical Research 115, F03017. doi:10.1029/2009JF001304.
Glotzbach, C., Bernet, M., van der Beek, P.A., 2011a. Detrital thermochronology records changing source areas and steady exhumation in the Western European Alps. Geology 39, 239–242. doi:10.1130/G31757.1.
Glotzbach, C., van der Beek, P.A., Spiegel, C., 2011b. Episodic exhumation and relief growth in the Mont Blanc massif, Western Alps from numerical modelling of thermochronology data. Earth and Planetary Science Letters 304, 417–430.
Green, P.F., Duddy, I.R., Gleadow, A.J.W., Tingate, P.R., Laslett, G.M., 1986. Thermal annealing of fission tracks in apatite 1. A qualitative description. Chemical Geology 59, 237–253.
Grove, M., Harrison, T., 1996. Ar diffusion in Fe-rich biotite. American Mineralogist 81, 940–951.
Hames, W., Bowering, S., 1994. An empirical evaluation of the argon diffusion geometry in muscovite. Earth and Planetary Science Letters 124, 161–167.
Harrison, T.M., Célérier, J., Aikman, A.B., Hermann, J., Heizler, M.T., 2009. Diffusion of ^{40}Ar in muscovite. Geochimica et Cosmochimica Acta 73 (4), 1029–1051.
Hawkesworth, C.J., 1976. Rb/Sr geochronology in the Eastern Alps. Contributions to Mineralogy and Petrology 54, 225–244.
Hejl, E., 1997. 'Cold spots' during the Cenozoic evolution of the Eastern Alps: thermochronological interpretation of apatite fission-track data. Tectonophysics 272, 159–173.
Hejl, E., 1998. Über die känozoische Abkühlung und Denudation der Zentralalpen östlich der Hohen Tauern — eine Apatit-Spaltspurenanalyse. Mitteilungen der Österreichischen Goelogischen Gesellschaft 89, 179–200.
Hergarten, S., Wagner, T., Stüwe, K., 2010. Age and prematurity of the Alps derived from topography. Earth and Planetary Science Letters 297, 453–460. doi:10.1016/j.epsl.2010.06.048.
Hoke, L., 1990. The Altkristallin of the Kreuzeck Mountains, SE Tauern Window, Eastern Alps; basement crust in a convergent plate boundary zone. Jahrbuch der Geologischen Bundesanstalt 133 87 pp.
Hourigan, J.K., Reiners, P.W., Brandon, M.T., 2005. U–Th zonation-dependent alpha ejection in (U–Th)/He chronometry. Geochimica et Cosmochimica Acta 69, 3349–3365.
Hurford, A.J., Green, P.F., 1983. The zeta age calibration of fission-track dating. Chemical Geology 41, 285–312.
Inger, S., Cliff, A., 1994. Timing of metamorphism in the Tauern Window, Eastern Alps: Rb–Sr ages and fabric formation. Journal of Metamorphic Geology 12, 695–707.
Jäger, E., Karl, F., Schmidegg, O., 1969. Rubidium–Strontium-Altersbestimmungen a Biotit–Muskowit — Granitgneisen (Typus Augen- und Flasergneise) aus dem nördlichen Großvenedigerbereich (Hohe Tauern). Mineralogy and Petrology 13 (2–3), 251–272.
Ketcham, R.A., 2005. Forward and inverse modeling of low-temperature thermochronometry data. In: Reiners, P., Ehlers, T.A. (Eds.), Low-temperature thermochronology: techniques, interpretations, and applications. : Rev. Mineral. Geochem., 58. Am. Mineral. Soc., Washington, D.C., pp. 275–314.
Kirschner, D., Cosca, M., Masson, H., Hunziker, J., 1996. Staircase 40Ar/39Ar spectra of fine-grained white mica; timing and duration of deformation and emperical constraints on argon diffusion. Geology 24 (8), 747–750.
Kissling, E., Schmid, S.M., Lippitsch, R., Ansorage, J., Fügenschuh, B., 2006. Lithosphere structure and tectonic evolution of the Alpine arc: new evidence from high-resolution teleseismic tomography. In: Stephenson, R.A., Gee, D.G. (Eds.), European lithosphere dynamics: Mem. Geol. Soc. London, 32, pp. 129–145.
Kralik, M., Klima, K., Riedmüller, G., 1987. Dating of fault gouges. Nature 327, 315–317. doi:10.1038/327315a0.
Kuhlemann, J., 2000. Post-collisional sediment budget of circum-Alpine basins (Central Europe). Memorie degli Istituti di Geologia e Mineralogia dell' Università di Padova 52, 1–91.
Kuhlemann, J., 2007. Paleogeographic and paleotopographic evolution of the Swiss and Eastern Alps since the Oligocene. Global and Planetary Change 58, 224–236.
Kuhlemann, J., Frisch, W., Dunkl, I., Székely, B., 2001. Quantifying tectonic versus erosive denudation by the sediment budget: the Miocene corcomplexes of the Alps. Tectonophysics 330, 1–23.
Kuhlemann, J., Frisch, W., Székely, B., Dunkl, I., Kázmér, M., 2002. Post-collisonal sediment budget history of the Alps: tectonic versus climatic control. International Journal of Earth Sciences (Geolog Rundsch) 91, 818–837.
Kurz, W., Neubauer, F., 1996. Deformation partitioning during updoming of the Sonnblick area in the Tauern Window (Eastern Alps). Journal of Structural Geology 18, 1327–1343.
Kurz, W., Fritz, H., Piller, W.E., Neubauer, F., Genser, J., 2001. Overview of the Paleogene of the Eastern Alps. In: Piller, W.E., Rasser, M. (Eds.), Paleogene of the Eastern Alps: Österr. Akad. Wiss. Schriftenr. Erdwiss. Komm., 14, pp. 11–56.
Kurz, W., Wölfler, A., Rabitsch, R., Genser, J., 2011. Polyphase movement on the Lavanttal Fault Zone (Eastern Alps): reconciling the evidence from different geochronological indicators. Swiss Journal of Geosciences 104 (2), 323–343. doi:10.1007/s00015-011-0068-y.
Lambert, R.St.J., 1970. A potassium–argon study of the margin of the Tauernfenster at Döllach, Austria. Eclogae Geologicae Helvetiae 63, 197–205.
Linner, M., Habler, G., Grasemann, B., 2008. Vom Defereggen-Antholz-Vals- (DAV) zum Pustertal-Gailtal-Störungssystem: Mehrphasige spröde Deformation im Ostalpinen Kristallin. Journal of Alpine Geology 49, 64–65.
Linzer, H.F., Moser, F., Nemes, F., Ratschbacher, L., Sperner, B., 1997. Build-up and dismembering of the eastern Northern Calcareous Alps. Tectonophysics 272, 97–124. doi:10.1016/S0040-1951(96)00254-5.
Linzer, H.G., Decker, K., Peresson, H., Dell'Mour, R., Frisch, W., 2002. Balancing lateral orogenic float of the Eastern Alps. Tectonophysics 354, 211–237. doi:10.1016/S0040-1951(02)00337-2.
Lippolt, H.J., Leitz, M., Wernicke, R.S., Hagerdon, B., 1994. (Uranium + thorium)/helium dating of apatite: experience with samples from different geochemical environments. Chemical Geology 112, 179–191. doi:10.1016/00009-2541(94)90113-9.
Lips, A.L.W., White, S.H., Wijbrans, J.R., 1998. ^{40}Ar/^{39}Ar laserprobe direct dating of discrete deformational events: a continuous record of early Alpine tectonics in the Pelagonian Zone, NE Aegean area, Greece. Tectonophysics 298, 133–153.
Liu, Y., Genser, J., Handler, R., Friedl, G., Neubauer, F., 2001. 40Ar/39Ar muscovite ages from the Penninic–Austroalpine plate boundary, Eastern Alps. Tectonics 20, 526–547. doi:10.1029/2001TC900011.
Luth, S.W., Willingshofer, E., 2008. Mapping of the post-collisional cooling history of the Eastern Alps. Swiss Journal of Geosciences 101 (1), 207–223. doi:10.1007/s00015-008-1294-9.
Lyon-Cean, H., Molnar, P., 1989. Constraints on the deep structure and dynamic processes beneath the Alps and adjacent regions from an analysis of gravity anomalies. Geophysical Journal International 89, 19–32.
Mancktelow, N.S., Stöckli, D.F., Grollimund, B., Müller, W., Fügenschuh, B., Viola, G., Seward, D., Villa, I.M., 2001. The DAV and Periadriatic fault systems in the Eastern Alps south of the Tauern Window. International Journal of Earth Sciences 90, 593–622.
McDowell, F.W., McIntosh, W.C., Farley, K.A., 2005. A precise ^{40}Ar-39^{Ar} reference age for the Durango apatite (U–Th)/He and fission-track dating standard. Chemical Geology 214, 249–263.
Mosar, J., 1999. Present-day and future tectonic underplating in the western Swiss Alps: reconciliation of basement/wrenchfaulting and decollement folding of the Jura and Molasse basin in the Alpine foreland. Earth and Planetary Science Letters 173, 143–155.
Most, P., 2003. Late Alpine cooling histories of tectonic blocks along the central part of the TRANSALP-traverse (Inntal-Gardertal): constraints from geochronology. Tübinger Geowissenschaftliche Arbeiten Reihe A 67 97 pp.
Müller, W., Mancktelow, N.S., Meier, N., 2000. Rb–Sr microchrons of synkinematic mica in mylonites: an example from the DAV fault of the Eastern Alps. Earth and Planetary Science Letters 180, 385–397.
Oxburgh, E.R., Lambert, R.St.J., Baadsgaard, H., Simons, J.G., 1966. Potassium–argon age studies across the southeastern margin of the Tauern Window, the Eastern Alps.
Purdy, J., Jäger, E., 1976. K–Ar ages on rock-forming minerals from the Central Alps. Memorie dell'Istituto della Regia Università di Padova 30, 31….
Ratschbacher, L., Merle, O., Davy, P., Cobbold, P., 1991a. Lateral extrusion in the Eastern Alps. Part 1: boundary conditions and experiments scaled for gravity. Tectonics 10, 245–256.
Ratschbacher, L., Frisch, W., Linzer, H.G., Merle, O., 1991b. Lateral extrusion in the Eastern Alps. Part 2: structural analysis. Tectonics 10, 257–271.
Reddy, S.M., Cliff, R.A., East, P., 1993. Thermal history of the Sonnblick Dome, south-east Tauern Window, Austria: implications for heterogeneous uplift within the Penninic basement. Geologische Rundschau 82, 667–675.
Reinecker, J., 2000. Stress and deformation: Miocene to present-day tectonics in the Eastern Alps. Tübinger Geowissenschaftliche Arbeiten Reihe A 55 128 pp.
Reinecker, J., Lenhardt, W.A., 1999. Present-day stress field and deformation in eastern Austria. Geologische Rundschau 88, 532–550.
Reiners, P.W., 2005. Zircon (U–Th)/He thermochronometry. Reviews in Mineralogy and Geochemistry 58, 151–179.
Reiners, P.W., Zhou, Z., Ehlers, T.A., Xu, C., Brandon, M.T., Donelick, R.A., Nicolescu, S., 2003. Post-orogenic evolution of the Dabie Shan, Eastern China, from (U–Th)/He and fission track thermochronology. American Journal of Science 303, 489–518.
Robl, J., Stüwe, K., 2005a. Continental collision within finite indenter strength 1: concept and model formulation. Tectonics 24. doi:10.1029/2004TC001727.

Robl, J., Stüwe, K., 2005b. Continental collision with finite indenter strength: 2. European Eastern Alps. Tectonics 24. doi:10.1029/2004TC001741.
Robl, J., Stüwe, K., Hergarten, S., Evans, L., 2008. Extension during continental convergence in the Eastern Alps: the influence of orogen-scale strike slip faults. Geology 36, 963–966. doi:10.1130/G25294A.1.
Rolland, Y., Corsini, M., Rossi, M., Cox, S.F., Pennacchioni, G., Mancktelow, N., Boullier, A.M., 2007. Comment on the dating of Alpine deformation by Ar–Ar on syn-kinematic mica in mid-crustal shear zones of the Mont Blanc Massif (paper by Leloup et al.). Tectonics 26, TC2015. doi:10.1029/2006TC001956.
Rolland, Y., Rossi, M., Cox, S.F., Corsini, M., Mancktelow, N., Pennacchioni, G., Fornari, M., Boullier, A.M., 2008. $^{40}Ar/^{39}Ar$ dating of syn-kinematic white mica: insights from fluid–rock reaction in low-grade shear zones (Mont Blanc Massif) and constraints on timing of deformation in the NW External Alps. In: Wibberley, C.A.J., Kurz, W., Imber, J., Holdsworth, R.E., Colletini, C. (Eds.), The internal structure of fault zones: implications for mechanical and fluid-flow properties: Geol. Soc. Spec. Pub., 299, pp. 293–315. doi:10.1144/SP299.17.
Rolland, Y., Cox, S.F., Corsini, M., 2009a. Constraining deformation stages in brittle–ductile shear zones from combined field mapping and 40Ar/39Ar dating: the structural evolution of the Grimsel Pass area (Aar massif, Swiss Alps). Journal of Structural Geology 31, 1377–1394. doi:10.1016/j.jsg.2009.08.003.
Rolland, Y., Galoyan, Gh., Bosch, D., Sosson, M., Corsini, M., Fornari, M., Vérati, C., 2009b. Jurassic Back-arc and hot-spot related series in the Armenian ophiolites — implications for the obduction process. Lithos. doi:10.1016//j.lithos.2009.02.006.
Rolland, Y., Lardeaux, J.-M., Jolivet, L., 2012. Deciphering orogenic evolution. Journal of Gedynamics 56–57, 1–6.
Rosenberg, C.L., Schneider, S., 2008. The western termination of the SEMP Fault (Eastern Alps) and its bearing on exhumation of the Tauern Window. In: Siegesmund, S., Froitzheim, N., Fügenschuh, B. (Eds.), Tectonic aspects of the Alpine–Dinaride–Carpathian system: Geol. Soc. London Spec. Publ., 298, pp. 197–218. doi:10.1144/SP298.100305.
Rosenberg, C.L., Brun, J.P., Cagnard, F., Gapais, D., 2007. Oblique indentation in the Eastern Alps: insights from laboratory experiments. Tectonics 26. doi:10.1029/2006TC001960.
Sanchez, G., Rolland, Y., Schneider, J., Corsini, M., Oliot, E., Goncalves, P., Verati, C., Lardeaux, J.-M., Marquer, D., 2011. Dating low-temperature deformation by $^{40}Ar/^{39}Ar$ on white mica, insights from the Argentera–Mercantour Massif (SW Alps). Lithos 125 (1–2), 521–536.
Schmid, S.M., Aebli, H.R., Zingg, A., 1989. The role of the Periadriatic Line in the tectonic evolution of the Alps. Geological Society Special Publication 45, 153–171. doi:10.1144/GSL.SP.1989.045.01.08.
Schulz, B., 1989. Jungalpidische Gefügeentwicklung entlang der Defereggen-Antholz-Vals-Linie (Osttirol, Österreich). Jahrbuch der Geologischen Bundesanstalt 132, 775–789.
Schumer, R., Jerolmack, D.J., 2009. Real and apparent changes in sediment deposition rates through time. Journal of Geophysical Research 114. doi:10.1029/2009JF001266.
Schuster, R., Stüwe, K., 2008. Permian metamorphic event in the Alps. Geology 36, 603–606.
Schuster, R., Scharbert, S., Abart, R., Frank, W., 2001. Permo-Triassic extension and related HT/LP metamorphism in the Austroalpine–Southalpine realm. Mitteilungen der Gesellschaft der Geologie und Bergbaustudenten in Oesterreich 45, 111–141.
Schuster, R., Koller, F., Hoeck, V., Hoinkes, G., Bousquet, R., 2004. Explanatory notes to the map: metamorphic structure of the Alps–metamorphic evolution of the Eastern Alps. Mitteilungen der Österreichischen Mineralogischen Gesellschaft 149, 175–199.
Selverstone, J., 1988. Evidence for east–west crustal extension in the Eastern Alps: implications for the unroofing history of the Tauern window. Tectonics 7, 87–105.
Selverstone, J., 2005. Are the Alps collapsing? Annual Review of Earth and Planetary Sciences 32, 113–132.
Staufenberg, H., 1987. Apatite fission-track evidence for postmetamorphic uplift and cooling history of the eastern Tauern Window and the surrounding Austroalpine (Central Eastern Alps, Austria). Jahrbuch der Geologischen Bundesanstalt 130, 571–586.
Stüwe, K., Hintermüller, M., 2000. Topography and isotherms revisited: the influence of laterally migrating drainage divides. Earth and Planetary Science Letters 184, 287–303.
Stüwe, K., White, L., Brown, R., 1994. The influence of eroding topography to fission track analysis. Earth and Planetary Science Letters 124, 63–74.
Thöni, M., 2006. Dating eclogite-facies metamorphism in the Eastern Alps — approaches, results, interpretations: a review. Mineralogy and Petrology 88, 123–148.
Vernon, A.J., van der Beek, P.A., Sinclair, H.D., Rahn, M.K., 2008. Increase in late Neogene denudation of the European Alps confirmed by isoage analysis of a fission-track database. Earth and Planetary Science Letters 270, 316–329.
Villa, I.M., 1998. Isotopic closure. Terra Nova 10, 42–47.
Viola, G., Mancktelow, N.S., Seward, D., 2001. Late Oligocene–Neogene evolution of Europe–Adria collision: new structural and geochronological evidence from the Giudicarie fault system (Italien Eastern Alps). Tectonics 20, 999–1020. doi:10.1029/2001TC900021.
Von Blanckenburg, F., Davies, J.H., 1995. Slab breakoff: a model for syncollisional magmatism and tectonics in the Alps. Tectonics 14, 120–131.
Von Eynatten, H., Schlunegger, F., Gaupp, R., Wijbrans, J.R., 1999. Exhumation of the Central Alps: evidence from $^{40}Ar/^{39}Ar$ laserprobe dating of detrital white micas from the Swiss Molasse Basin. Terra Nova 11, 284–289.
Wagner, G.A., Van den haute, P., 1992. Fission-Track Dating. Enke Stuttgart. 285 pp.
Wagner, T., Fabel, D., Fiebig, M., Häuselmann, P., Sahy, D., Xu, S., Stüwe, K., 2010. Young uplift in the non-glaciated parts of the Eastern Alps. Earth and Planetary Science Letters 295, 159–169. doi:10.1016/j.epsl.2010.03.034.
Wang, X., Neubauer, F., 1998. Orogen-parallel strike-slip faults bordering metamorphic core complexes: the Salzach–Enns fault zone in the Eastern Alps, Austria. Journal of Structural Geology 20, 799–818. doi:10.1016/S0191-8141(98)00013-3.
Waters, D.J., 1976. Structural, metamorphic and geochronological studies in the south east Tauern Window. Unpublished PhD Thesis, University of Oxford.
Willenbring, J.K., Blanckenburg, F.V., 2010. Long term stability of global erosion rates and weathering during late-Cenozoic cooling. Nature 465, 211–214. doi:10.1038/nature09044.
Willett, S.D., 2010. Late Neogene erosion of the Alps: a climate driver? Annual Review of Earth and Planetary Sciences. doi:10.1146/annurev-earth-040809-152543.
Willett, S.D., Schlunegger, F., Picotti, V., 2006. Messinian climate change and erosional destruction of the European Alps. Geology 34, 613–616.
Winkler-Hermaden, A., 1957. Geologisches Kräftespiel und Landformung. Springer Verlag, Vienna. 822 pp.
Wolf, R.A., Farley, K.A., Silver, L.T., 1996. Helium diffusion and low temperature thermochronometry of apatite. Geochimica et Cosmochimica Acta 60, 4231–4240.
Wölfler, A., Dekant, C., Danišík, M., Kurz, W., Dunkl, I., Putiš, M., Frisch, W., 2008. Late stage differential exhumation of crustal blocks in the central Eastern Alps: evidence from fission track and (U–Th)/He thermochronology. Terra Nova 20, 378–384.
Wölfler, A., Kurz, W., Danišík, M., Rabitsch, R., 2010. Dating of fault zone activity by apatite fission track and apatite (U–Th)/He thermochronometry: a case study from the Lavanttal fault system (Eastern Alps). Terra Nova 22, 274–282.
Wölfler, A., Kurz, W., Fritz, H., Stüwe, K., 2011. Lateral extrusion in the Eastern Alps revisited: refining the model by thermochronological, sedimentary and seismic data. Tectonics 30, TC4006. doi:10.1029/2010TC002782.